Alisawi A.T., Collins P.E.F., Cashell K.A. Nonlinear Numerical Simulation of Physical Shaking Table Test using Three Different Soil Constitutive Models. Accepted for publication in Soil Dynamics and Earthquake Engineering, 2021. Available at:

Nonlinear Numerical Simulation of Physical Shaking Table Test, Using Three Different Soil Constitutive Models

Alisawi A. T.[a*], Collins P. E. F.[b*], and Cashell K. A.[c*]

*Department of Civil and Environmental Engineering, Brunel University London, UK

[a] Alaa.Al-Isawi@brunel.ac.uk, [b] Philip.Collins@brunel.ac.uk, and [c] Katherine.Cashell@brunel.ac.uk

Corresponding author, Alaa Alisawi, Howell Building 302, Kingston Lane, London, Uxbridge UB8 3PH

Mobile:0044(0)7399439443

Abstract

Dynamic response records of pile performance during earthquakes are limited mainly due to the challenges of recording the seismic soil–pile response. This limitation has led to an inadequacy in providing a standardized basis for the calibration and validation of the available analytical and numerical methods developed for seismic soil–pile superstructure interaction problems. To bridge this gap, a series of numerical simulations of scaled, shaking table tests of model piles in soft clay has been developed in the current study. This paper aims to accurately identify all aspects and critical parameters in the numerical simulation and propose the most suitable soil constitutive model. Three soil constitutive models are selected as advanced models for soft soil, namely, the modified Mohr–Coulomb, Drucker–Prager/cap plasticity, and Cam–clay models. Similar to the physical test case study, this numerical analysis uses dimensional analysis techniques to identify scale modelling criteria and develop a scaled soil and pile-supported structure model correctly. The 3D nonlinear numerical models are developed using the Abaqus software.

Keywords: Seismic soil-structure interaction; Mohr–Coulomb model; Drucker–Prager/cap plasticity model; Cam–clay model, Shaking table; Finite element analysis; Abaqus.

1. Introduction

Seismic soil-structure interaction (SSI) analysis is a sophisticated process that simultaneously involves pore water pressure generation, ground and foundation/pile deformation and a gap-/slap mechanism. In traditional seismic design, the effect of the pile on the ground motions applied to the structure is typically ignored or simplified to facilitate the analyses [1-3]. This practice is generally accepted as a conservative design hypothesis for spectral analysis because flexible pile foundations lengthen the natural period of the structure and increase the damping provided [2]. Moreover, SSI effects are presumed advantageous during earthquake excitation because they can increase the structural flexibility and natural period of the structure and consequently decrease the base shear forces. Simplified and non-standardised analyses are widely used to assess pile integrity during seismic loading [3].

Two of the most relevant discussions currently in SSI research are (i) increasing residual deformations and (ii) decreasing the stiffness of the pile foundation system, which in turn may affect the seismic response and structural displacement [6]. The ground motions experienced by a superstructure are influenced by the pile system, and piles may experience extreme damage and/or failure under earthquake loading. In general, there is insufficient information in the public domain regarding seismic soil–pile response cases, and several of the cases that are published only involve piles equipped to record the dynamic response. These cannot provide a reliable basis for calibrating and validating the analytical techniques which have been developed for seismic soil–pile–superstructure interaction (SSPSI) problems.

In this context, in recent years researchers have been conducting centrifuge and shaking table tests under controlled laboratory conditions. The majority of these tests have investigated seismic responses in

cohesionless soils with liquefaction potential [4]. However, many piles are located on soft clays that have the potential for cyclic strength degradation during seismic loading [7-9]. Therefore, the need for a greater research focus into SSPSI is clear. Laboratory shaking table tests on specimens with a flexible wall offer an opportunity to extend the limited performance data of SSPSI in soft clays, under various controlled test conditions [7]. The flexible wall container allows the soil to move horizontally along the depth and therefore this test method can provide a realistic response compared with those using other types of container [8]. Moreover, these experiments can fully represent the coupled behaviour of the soil–pile–superstructure system.

In the past, the majority of numerical soil-pile/foundation models presented in the available literature have employed a Winkler spring model, which uses beam elements to represent the pile, spring elements for the soil along the pile surface that is embedded in the ground, and applied earthquake time history at the bottom of the structure or at the side boundary condition [9]. The wave propagation and output data are unrealistic however as the soil model is usually restricted to being either linear elastic or viscoelastic, owing to the limitations of finite element analysis (FEA) and computer resources. Moreover, to apply the nonlinear FEA approach in engineering practice, the resulting numerical simulations should be further verified through experiments [10]. Zhang et al. [11] described the damping characteristics of the soil–structure system using physical shake table tests. The study observed that the predominant period and the system mode shape tend to be compatible, the amplitude of transfer function rises, the interface motion state is coordinated, and the modal damping ratios are identical. The SSI system can be considered as the engineered classical damping mechanism by selecting a dynamic analytical approach in practical projects. Yang et al. [12] captured the effect of SSPSI on the dynamic behaviour of structure and soil by employing two groups of large-scale shaking table tests of 12 storey RC frame-founded pile group embedded in soft soil for two different test conditions, considering the SSI effect. The results revealed that SSPSI amplifies the storey drift and peak displacements. However, the peak acceleration and base shear force of the structure were reduced. It was recommended that the SSI must be realistically considered in order to provide an accurate seismic design for structures on soft soils.

Chen et al. [13] investigated the effect of seismic excitation on the behaviour of granular landslides subjected to horizontal and vertical seismic motion using a small-scale shaking table model test. The results demonstrated that the soil deposit shape is affected significantly by the motion frequency characteristics, where the maximum measured displacement of the system increases with the natural frequency for both the horizontal and vertical applied motion scenarios. The slope and sidewall angles of the landslide deposits are examined under different seismic waves in order to provide preliminary guidelines for the design of protective structures. Zhang et al. [14] studied the soil-structure interaction system and seismic behaviour of double box utility tunnels with joint-connections using shaking table model tests. The input motion in this study was an earthquake with a scaled PGA of 0.2 g, 0.4 g, 0.8 g or 1.2 g. Moreover, in order to examine the influence of frequency characteristics on the seismic behaviour, a series of artificial sine waves with a PGA of 0.2 g and five different frequencies ranging between 5-30 Hz were also examined as a second group of input motions. The study revealed that the effect of soil-structure interaction on the seismic behaviour of this system is significantly greater when the PGA value of the input motion is increased. The acceleration response of the system is considerably affected by the dynamic property of the soil, such as dynamic shear strain and damping ratio. The motion frequency content was shown to have a significant effect and therefore the recommendation was that a natural frequency should be used when the utility tunnel is under construction.

One of the key challenges in modelling geotechnical materials is representing the dynamic response of the soil accurately under various external loading conditions. Soil materials can have a range of diverse and complex properties, including their elasticity, viscosity and plasticity. Nevertheless, reliable constitutive models are capable of simulating the material as a complex, heterogeneous and strongly nonlinear material [15] for various soil types and conditions, such as cohesive or non-cohesive and saturated or unsaturated soils [16]. Dynamic response records of co-seismic pile performance are limited due to complexities and a lack of well-documented soil–pile response case histories. These limitations lead to inadequate provision of a standardised basis for the calibration and validation of the methods developed for seismic soil–pile superstructure interaction (SSPSI) problems. To address this, a series of numerical simulations (using finite element analysis (FEA)) for shaking table tests of scaled model piles in soft clay has been developed. The study identifies all numerical simulation aspects and soil constitutive criteria successfully. The shaking table test programme developed by Philip Meymand has been adopted as a physical test case. The study uses dimensional analysis to identify scale modelling criteria and develop a scaled soil and pile-supported structure model correctly. A unique numerical methodology is designed to permit multi-directional shear deformations, minimise boundary effects and replicate the free-field site response. Soil–structure interaction (SSI) effects, including the gap/slap mechanism and the consequences of kinematic and inertial force, are clearly shown. In this context, the current paper is focussed on the development of a three-dimensional (3D) finite element (FE) model to simulate a physical shaking table test with a flexible wall barrel, to simulate the dynamic response of a soil structure interaction system founded in a soft clay. The paper proceeds with a description of the shaking table tests which are later employed to validate the numerical analysis [17]. This is followed by a detailed description of the finite element model, which is developed using the Abaqus software [18]. The model is then employed to further understand the behaviour.

2. Reference case

A series of physical shaking table tests comprising flexible wall barrel containers were conducted by Meymand et al. at the UC Berkeley PEER Centre Earthquake Simulator Laboratory [17], and the data from these experiments are employed herein for validation of the numerical modelling. The principal objectives of the physical shaking table tests were to achieve insights into SSPSI behaviour modes and produce a set of performance data, which could then be employed for further analysis. Two specimens from Phase II of this study are selected as reference cases for the current work, namely tests 1.15 and 2.26. Both of these comprised soil which was embedded with a single pile supporting the superstructure. The experimental set-up was able to physically model the entire seismic soil–pile–superstructure interaction (SSPSI). The main aim of the experimental campaign was to provide an insight into specific SSPSI issues, such as the frequency response of the structure, multidirectional excitation, kinematic and inertial responses and pile/cap soil contact.

The individual model piles were tested simultaneously and arranged in the test container in a manner that minimised element interactions [19]. In terms of instrumentation, there were twenty-three accelerometers arranged in two vertical arrays embedded in the soil deposit, which were attached to the head masses of the piles (i.e., the superstructure) to capture translation and rocking motions. In addition, seven pairs of strain gauges were attached to each pile. Based on the soil strength and shear wave velocity profiles, the soil in the tests was defined as being lightly over-consolidated soft to medium stiff clay.

2.1. Scale modelling

As with all shaking table tests, the scaling details are very important and the relationship between the scale model and the desired full-scale prototype behaviour requires careful consideration. Kline [20] defined three approaches for enhancing the power and complexity for scale modelling applications: dimensional analysis,

similitude theory and governing equations. However, none of these approaches in isolation is capable of representing the true behaviour of this highly nonlinear and complex scenario. Therefore, in the physical experiments [17], a combined scaling method system was developed by identifying and modelling the primary forces and processes in the system whilst suppressing minor effects. Considering the complexity of the SSPSI problem and the significance of the approach for defining the variables and modes of the system, the scaling method was designed to capture the behaviours of the principal interests adequately. The accuracy of this combined scaling method was classified as being either "distorted", "adequate" or "true" depending on the degree of precision required for a particular scenario [21].

In the current study, this combined method is applied to create a "true" model that can represent all primary parameters that are involved in the SSPSI mode in the produced scaled model. All primary parameters of the prototype elements, i.e. the soil and the piles, are demonstrated in dimensional form using an appropriate scaling factor. Table 1 summarises the main model parameters defined in terms of the geometric scaling factor (λ) employed in this study, where *EI* is the product of the Young's modulus (E) and the second moment of area for the section (I). The geometric scaling factor employed in the reference case had a value equal to 8 [17], and therefore this value is also adopted in the current study.

Table 1. Geometric scaling factor λ [17]

Variable	Factor	Variable	Factor
Mass Density	1	Force	λ^3
Acceleration		EI	λ^5
Strain		Frequency	$\lambda^{-\frac{1}{2}}$
Length	λ	Stiffness	λ^2
Stress		Time	$\lambda^{\frac{1}{2}}$
Modulus		Velocity	

2.2. Details of the physical shaking tests

The shaking table employed in these physical tests was 6.1 m × 6.1 m in plan, and had a load capacity of 580 kN, a frequency range of 0–20 Hz and six controlled degrees of freedom [4]. In geotechnical scaled modelling, a container is typically utilised to confine the soil and to impose boundary conditions that may not occur in the prototype full-scale field scenario. Accordingly, in these tests, a suitable container was designed that could minimise the effect of free boundary conditions on the overall system response and also enable the model to replicate the seismic behaviour at the level ground (i.e. the free field). On this basis, a laterally flexible and radially stiff cylindrical container was selected for the quasi-free field response. This design extends the centrifuge testing laminar box concept to permit multi-directional excitation [22].

The container constrained a soil column which was 2.3 m in diameter and 2.0 m in height and installed on the surface of the shaking table, as shown in Fig. 1. The top steel ring was supported by four steel pipe columns connected by heavy-duty universal joints, which allowed the ring full translational freedom but prevented overturning rotations. The flexible wall of the container comprised a neoprene rubber membrane that was 6.4 mm thick, which was suspended from the top ring and fastened at the base. The flexible wall was confined by a set of woven Kevlar straps which were 45 mm in width and arrayed in circumferential bands around the exterior of the membrane and arranged at intervals of 60 mm. The elastic modulus (E) of

the combined membrane was designed to be identical to that of the soil to ensure that the free-soil boundary condition was not affected. The combination of the rubber membrane and the set of straps provided lateral flexibility and radial stiffness for the container boundary conditions. A plastic sheet sealed the top of the soil specimen during the period between tests, and water was sprayed on top of the soil to prevent the soil surface from drying out. For each test series, the pile was driven into the soil. After each test, the test arrangement was dismantled by removing the piles and backfilling the hole with soil. However, a new pile was driven into the soil the following day in order to perform the next test. The model was left approximately five days before performing the next test due to the beneficial effects of soil thixotropy.

Figure 1 Full scale container mounted on the shaking table, with support struts and soil mixer/pump in the background [17]

2.3. Soil model

A soil specimen with appropriately scaled stiffness and strength properties was developed for the physical test programme [17]. This model consisted of a weight percentage of 72% kaolinite, 24% bentonite and 20% type C fly ash. The shear wave velocity was measured at a water content of 130% and cure time of 5 days.

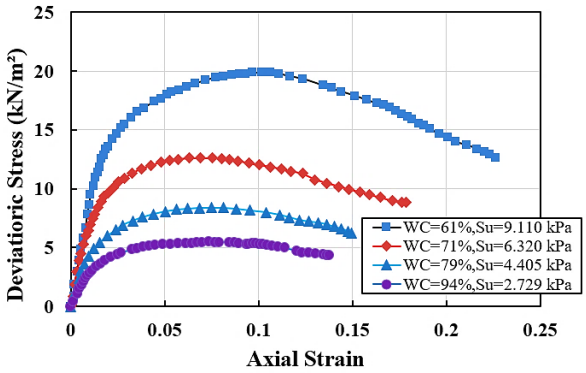

Figure 2. Unconsolidated-Undrained Triaxial compression test results for model soil mixture with 20% fly ash at 94% water content (adapted from [17])

A series of unconsolidated, undrained triaxial compression (UUTX) tests on scale model samples with 20% fly ash as a percentage of dry weight was conducted and the results reported in the reference case study [17]; these values were used to identify the numerical properties of soil constitutive models in the current study, and Fig. 2 shows that the shear strength of the undrained soil model S_u is dependent on the specimen water content. In the current study, a value of 94% water content is used in the soil model.

The property values used in the model, given the geometric scale factor of 8, are a static undrained shear strength of 25 kN/m^2 with a correction factor of the dynamic strength equal to 0.75 and a shear wave velocity of 111 m/sec. These values are consistent with Dickenson's equation [19]. Accordingly, the model soil constituted an "adequate" scale model of higher plasticity soft to medium stiff clay, such as San Francisco Bay mud. Table 2 represents the material soil properties for the full-scale prototype and the model used in the shaking table tests.

Table 2. Soil Properties for Prototype and Model

Parameters	**Prototype**	**Model**
Density (kg/m^3)	1505.7	1505.7
Undrained shear strength S_u (kN/m^2)	25	4.8
Elastic modulus E (kN/m^2)	33600	4200
Poisson's ratio	0.49	0.49
Shear wave velocity (m/sec)	111.0	39.6
Water content (%)	94	94
Liquid limit (%)	115	115
Plastic limit (%)	40	40
Plasticity index (%)	75	75
Rayleigh damping (%)	5	5

2.4. Pile model

In the full-scale prototype structure that was scaled and replicated in the shaking table tests [17], the pile comprised a steel pipe which was 410 mm in diameter (d) with a wall thickness of 12.7 mm (t_{wall}) and was filled with concrete, in accordance with the California Department of Transportation Highway Design Manual [23]. The scaling limitations described earlier resulted in a maximum prototype pile length of 12.8 m, thereby giving a pile length to diameter (L/d) ratio of 33, which is acceptable for a slender pile [9]. The stability conditions of the pile, which are crucial in terms of the lateral response, required that the pile should be fixed against rotation at the top and also relative displacement or translation at the base. The flexural rigidity of the pile was determined as 75.2 kN/m^2. The scaled model pile used in the shaking table tests was designed with due consideration given to the scaling limitations and hence a 6061 T-6 aluminium tube with a diameter (d) of 50.8 mm and wall thickness (t_{wall}) of 0.7 mm was employed. The pile provided an appropriate scaled flexural rigidity (EI) of 2.4 kN/m^2 and a L/d ratio of 36. Table 3 lists the properties of the pile for both the prototype and the model, including E_s, E_c and E_{pile} which are the elastic moduli for the steel, concrete and pile model (made from aluminium), respectively, G_{soil} is the shear modulus of the soil and EI_{comp} is the flexural stiffness of the steel and concrete section.

Table 3 Pile properties for the prototype and the model

Parameters	**Prototype**	**Model**
Outer diameter d (mm)	406.4	50.8
Wall thickness t_{wall} (mm)	12.7	0.7

Length L (m)	13.4	2.3
E_s (kN/m^2)	2.0×10^8	-
E_c (kN/m^2)	2.8×10^7	-
E_{pile} (kN/m^2)	-	6.9×10^7
L/d	33	36
d/t_{wall}	32	71.4
E_{pile}/G_{soil}	1392	3840
EI_{comp} (kN/m^2)	75.2	2.4
Rayleigh damping (%)	5	5

3. Development of the numerical model

The finite element model was developed using the Abaqus software [18], implementing the data from Phase II of the shaking table tests previously described [17]. Tests 1.15 and 2.26 from that test programme are selected for the validation, and these specimens had a flexible wall barrel container, and adopted a single pile model arrangement. More details on the representation of these tests in the numerical model are presented hereafter.

3.1. Input into the numerical model

In Test 1.15, a set of single pile models with head masses of 3.0, 11.40, 45.4 and 72.70 kg were examined whilst Test 2.26 studied free field models; both tests were subjected to unidirectional shaking. Similar to the shaking table tests loading condition, two levels of excitation are applied in the numerical model, namely medium and high excitations of the peak ground acceleration (PGA) corresponding to 0.2 g and 0.69 g, respectively. The input is taken from two different seismic events: (i) the 90 degree component from the Yerba Buena Island record during the Loma Prieta Earthquake (YBI90), and (ii) the Port Island station corresponding to the 79 m record north 00 east component during the Kobe Earthquake (KPI79N00). The YBI90 record had a predominant period of 0.67 sec, a time step of 0.02 sec and a PGA of 0.07 g, which for this physical and numerical testing programme was scaled to 0.2 g to provide the medium level of excitation. The KPI79N00 record had a predominant period of 0.345 sec, a time step of 0.01 sec and a PGA of 0.69 g, which was scaled to 0.7 g for the high level of excitation [24]. In accordance with the scaling relations given in Table 1, the time steps of these two records were divided by $\lambda^{0.5}$ in the both physical and numerical model, resulting in compressed time scales compared with the original records. The acceleration time histories, and acceleration response spectra for these two records, are shown in Fig. 4.

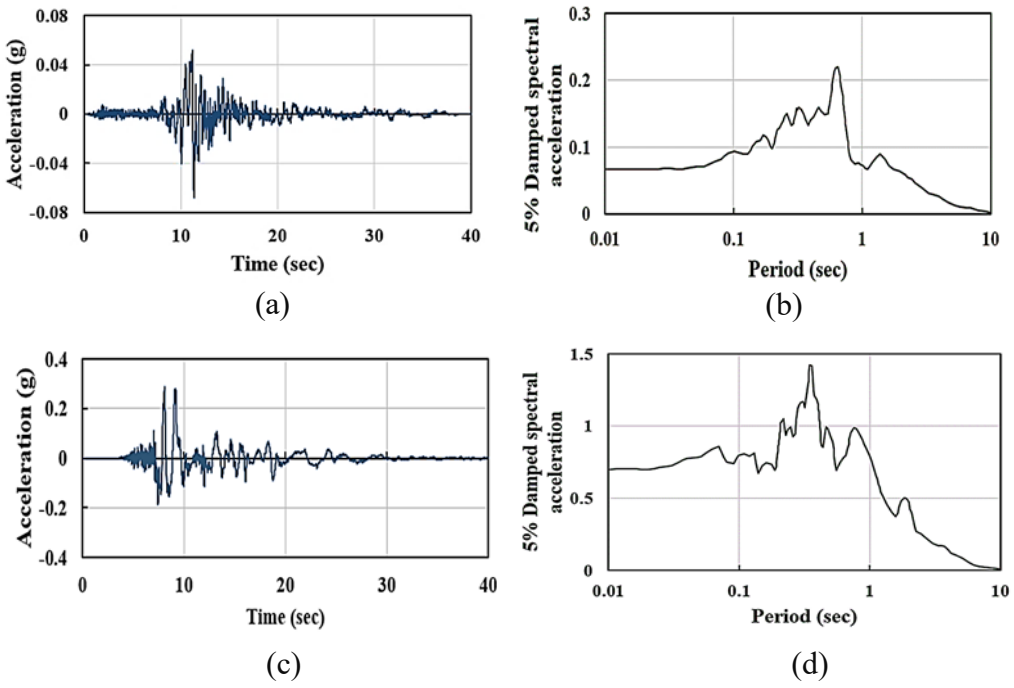

Figure 4. Input motions including (a) acceleration for YBI90, (b) acceleration response spectra for YBI90, (c) acceleration for the KPI79N00 and (d) acceleration response spectra the KPI79N00 [24]

3.2. Solution procedure, mesh and boundary conditions

A 3-dimensional finite element analysis is carried out in Abaqus using the sequential analysis method, which is capable of modelling the SSI under geostatic, static and dynamic loading. The different steps in the analysis are outlined hereafter:

(i) First is the geostatic step, in which only the soil body force is included. Consequently, the forces and initial stresses must be precisely established and equilibrated for minimal soil displacement [25].
(ii) This is followed by the first loading stage of the analysis, to create stability between the soil and the pile and prevent negative shear stress between them. This represents the piles' installation stage during model construction [26].
(iii) Then, the static-friction loading step is employed for the application of gravity loads, which are assumed to be static and uniform, in accordance with the loading conditions in the reference case study.
(iv) Next is the dynamic analysis step in which the time history input data are applied to the bottom of the clay soil (at the base of the shaking table) [27].

The displacements were restrained in the horizontal direction for the geostatic and static step and changed to the vertical direction allowing in this step, allowing free movement in the horizontal direction. The base of the model is restrained with roller supports in the vertical direction. By contrast, the other two direction boundary conditions, which are perpendicular to shaking direction, are constrained [28]. Both the soil and the superstructure are modelled using 3D solid elements (C3D8R in the Abaqus library) which are eight-node linear brick elements with reduced integration. For the piles, linear shell elements (S4R) are used, which are a four-node doubly curved shell elements [18], as shown in Fig. 5. As this is a cylindrical application, a radial mesh is employed in accordance with the approach of other researchers [29]. In addition, a mesh sensitivity study was conducted to achieve accurate and reliable results, resulting in which are 50 mm in each dimension at the boundary of the model and refined to 10 mm near and at the pile. The piles were simulated individually as this was found to give the most accurate results. Given the similarity between

the approach of using the combination system of flexible wall material properties, which was chosen in the reference case study, and the alternative method of using the soil sample properties directly, the combination system was not adopted further in the numerical analysis. Alternatively, the soil boundary was constrained in accordance with the physical test conditions.

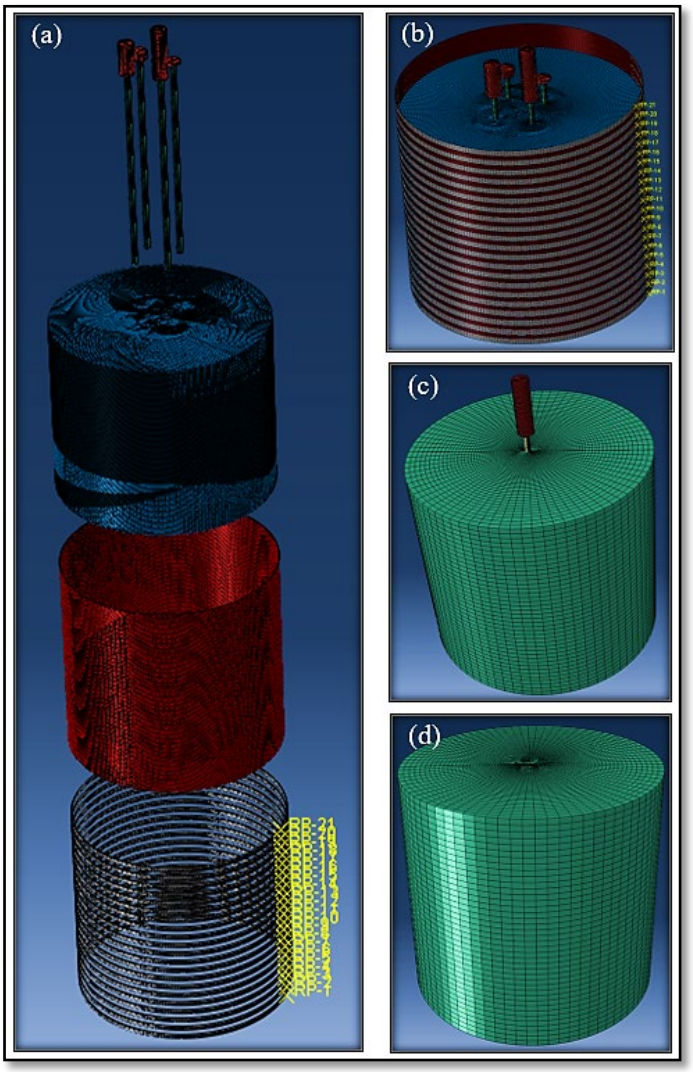

Figure 5. Images from the numerical simulation, including (a) the model assembly with the all component parts (b) meshing of the assembly of case (a), (c) the alternative solution of the boundary constrained condition in the finite element models, and (d) the free field model of the alternative solution

The geometric as well as the material nonlinearity is considered in the numerical simulation. Indeed, the geometric nonlinearity is critically based on setting the time incrementation parameters properly. Abaqus/Standard automatically modifies the size of the load increments so that it solves nonlinear problems successfully and efficiently. Only the size of the first increment in each step of the simulation have been identified. Therefore, a reasonable initial increment size should be provided. Automatic incrementation with the limitation of maximum displacement change of 0.1 is adopted. Direct method as an equation solver using asymmetric matrix storage and 'full newton' as solution technique is used in the geostatic step. For static steps, damping factor is specified as 0.0002 for the stabilization of unstable problems employing adaptive stabilization with maximum ratio of stabilization to strain energy of 0.05. Automatic incrementation type is applied. Direct method as an equation solver using asymmetric matrix storage and full newton as solution technique is employed. Abaqus presumes that external parameters, such as loads and boundary conditions, are either constant–step function or vary linearly ramped over a step. However, the appropriate option must

be selected depending on the analysis procedure. Ramp linearly over static step option is thus used in the current study. In dynamic step, automatic incrementation type is applied with default maximum increment size. An asymmetric matrix storage and full newton as solution technique is employed. Ramp linearly over dynamic step option, default time integrator parameter and initial acceleration calculation at the beginning of dynamic step are used in this analysis step.

3.3. Simulation of the soil–pile–superstructure interaction (SSPSI)

One of the most challenging issues in the numerical modelling of soil-structure interaction, and in particular seismic soil–pile–superstructure interaction (SSPSI), is accurate simulation of the contact between the piles and the surrounding soil. There are a number of different stress components including normal, tangential and relative surface sliding stresses as well as frictional shear stresses. In the numerical model, this contact is considered to be a discontinuous constraint, which can occur when loads transfer between contacting elements under contact conditions. In this case, once the two surfaces detach, the constraint is removed (i.e., the gap condition), and the slap condition takes place during the return of the contact. Abaqus includes two different formulations for modelling this scenario: (i) a small sliding formulation with limited sliding and some arbitrary rotation of the contact surfaces and (ii) a finite sliding formulation with separation and sliding of finite amplitude and some arbitrary rotation of the contact surfaces. In the case of the laterally loaded pile, the relative surface motion is categorised as small sliding. To model the normal behaviour, the 'hard contact' option is selected in the model as a contact property for defining the pressure-clearance relation. Moreover, the model removes the contact constraint when the value of the contact pressure becomes zero or less.

Contact surfaces in dynamic circumstances usually transmit normal and shear forces along with their contact interface. The Coulomb friction model, which is included in Abaqus, defines the interaction relation between the constraint surfaces which are in contact. In this study, both the static and kinematic friction coefficients of 0.61 and 0.47, respectively, are considered directly and the model identifies the exponential decay relation between the static and kinematic values. Accordingly, both normal and tangential behaviours are considered. Normal behaviour enables the pressure to transmit between the soil and the pile and both surfaces are in contact. This type of behaviour allows the soil to separate when the contact pressure reduces to zero. On the other hand, tangential behaviour enables the shear stress (or shear drag) to transfer between the soil and the pile surface, as shown in Fig.6.

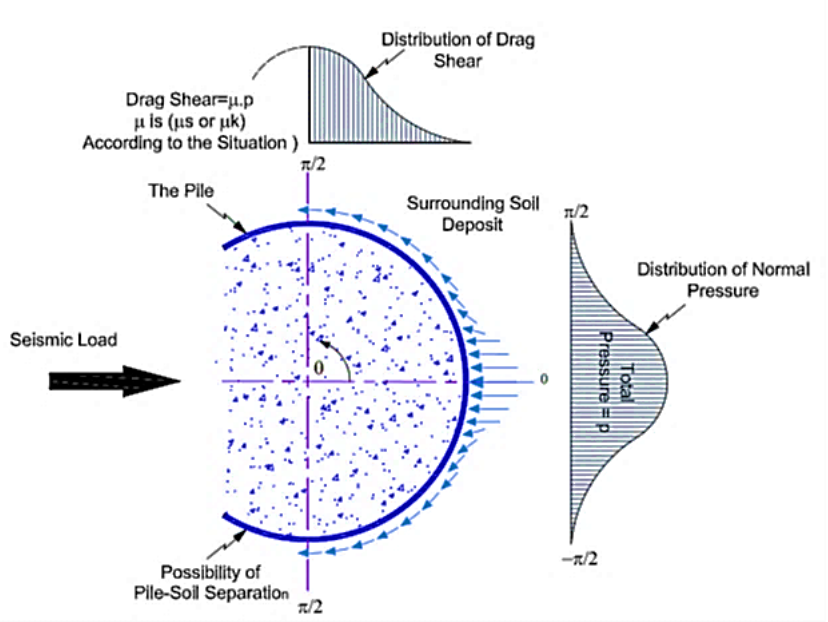

Figure 6. Schematic of normal pressure and drag-force distribution

3.4. Soil constitutive model

Soil is a heterogeneous material, and its behaviour is substantially affected by a variety of geotechnical and geological parameters, such as particle size and structure, mineralogy, pore water pressure and initial stress state. It is characterised by time-dependent behaviour (i.e. soil creep), and also includes many rheological aspects [30]. Over the past five decades, there have been many developments in the modelling of the stress–strain behaviour of soil [31]. These models are used to represent the soil behaviour in finite element and/or finite difference approaches of the soil–structure interaction problem under axisymmetric, plane strain and/or general 3D conditions. Simple and advanced models have been developed using the fundamental principles of soil mechanics and their complexity and accuracy can be categorised using experimental evidence or/and theoretical principles. The capabilities and shortcomings of these models can be arduous to determine, and choosing which model is most appropriate for a particular application is challenging. Therefore, the selection of an appropriate soil model relies on many parameters, such as soil type, problem category, solution procedure, complexity, and level of accessibility of the required parameters. For this reason, the current paper includes a detailed analysis of three of the most relevant models, including:

1. The Mohr–Coulomb model, which is commonly used for soil, both for static and monotonic dynamic loading conditions due to its clarity and the case with which the modelling parameters are defined. It is a linear elastic–perfectly plastic model;
2. The Drucker–Prager cap model is also very popular amongst the research community owing to its accurate depiction of the behaviour, and because it simulates a nonlinear elastic–hardening plastic response; and
3. The Cam–Clay model which is the newest of these three common approaches and also adopts a nonlinear elastic–hardening plastic response.

A fully nonlinear dynamic soil–structure interaction analysis with the application of the gap-slap mechanism is implemented in the current model and the capability of these three constitutive models for modelling the dynamic soil–structure interaction is assessed through comparisons with the physical shaking table experimental results.

3.4.1. Mohr–Coulomb model

In the standard version of Abaqus [18], the Mohr–Coulomb criterion assumes that soil failure happens once the shear stress in the soil reaches a specific value, which depends linearly on the normal stress in the failure plane. This model criterion is based on Mohr's circle of stress states at failure in the plane of the maximum and minimum principal stresses [32]. However, for general stress states, the criterion is conveniently expressed in terms of three invariant stresses, as given in Eq. 1:

$$F = R_{mc} q - p \tan \emptyset - c = 0, \qquad (1)$$

where $R_{mc}(\theta, \emptyset) = \frac{1}{\sqrt{3}\cos\emptyset} \times \sin\left(\theta + \frac{\pi}{3}\right) + \frac{1}{3}\cos\left(\theta + \frac{\pi}{3}\right)\tan\emptyset.$

The friction angle of the soil ($\emptyset$) denotes the slope of the Mohr–Coulomb yield surface in the $P - R_{mc}q$ stress plane, as shown in Fig.7, and depends on the following predefined field variables: θ is the deviatoric polar angle, p is the equivalent pressure stress, q is the Mises equivalent stress, r is the third invariant of deviatoric stress, ϕ the angle of internal friction and S is the deviatoric stress, which is described as a function of the normal stress σ, and the soil cohesion c [18].

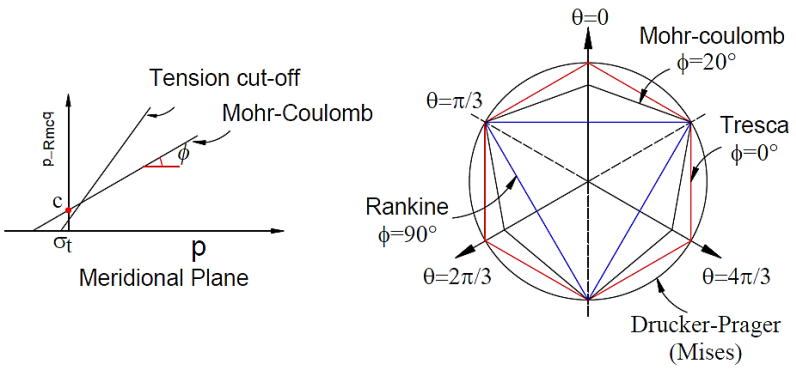

Figure 7. Mohr–Coulomb and tension cut-off surfaces in meridional and deviatoric planes (Modified from [18])

The shape of the yield surface in the deviatoric plane is controlled by the friction angle ∅, which ranges between $0° \leq \emptyset \leq 90°$. For $\emptyset = 0°$, the Mohr–Coulomb model cuts to a perfectly hexagonal deviatoric section−pressure independent Tresca model. For $\emptyset = 90°$, it reduces to the tension cut-off Rankine model—a triangular deviatoric section with $R_{mc} = \infty$—which is unsupported by the Mohr–Coulomb model in Abaqus. However, Abaqus/Standard sets the output variables as SP1, SP2 and SP3, corresponding to the principal stresses σ_1, σ_2 and σ_3, respectively.

Following the proposal of Mentrey and Willam (1995) [33], the hyperbolic function is adopted to represent the flow potential G in the meridional stress plane and smooth elliptic function in the deviatoric stress plane, as given in Eq. 2:

$$G = \sqrt{(\epsilon c_0 \tan\psi)^2 + (R_{mw} q)^2} - p \tan\psi \qquad (2)$$

where:

$$R_{mw}(\theta, e) = \frac{4\left(1-e^2\right) cos^2\theta + (2e-1)^2}{2(1-e^2)\cos\theta + (2e-1)\sqrt{4(1-e^2)\, cos^2\theta + 5e^2 - 4e}}\, R_{mc}\left(\frac{\pi}{3}, \emptyset\right),$$

$$R_{mc}\left(\frac{\pi}{3}, \emptyset\right) = \frac{3-\sin\emptyset}{6\cos\emptyset},$$

In these expressions, ψ is the dilation angle measured in the $p - R_{mw} q$ plane at high confining pressure and it can be predefined field variables dependent; c_0 is the initial cohesion yield stress; ϵ is the meridional eccentricity parameter, which defines the rate at that the hyperbolic function reaches the asymptote; and e is the deviatoric eccentricity parameter. In Abaqus, a default value of 0.1 is given for the meridional eccentricity ϵ, and the deviatoric eccentricity e is computed by default in accordance with Eq. 3:

$$e = \frac{3-\sin\emptyset}{3+\sin\emptyset}. \qquad (3)$$

This procedure matches the flow potential to the yield surface in both triaxial tension and compression in the deviatoric plane. Alternatively, Abaqus considers this deviatoric eccentricity as an independent material parameter by providing its value directly. The flow potential, which is continuous and smooth, ensures that the flow direction is consistently explicitly defined. Flow in the deviatoric stress plane is always non-associated. However, the flow in the meridional stress plane can be consider as associated flow in the condition that the angle of friction ∅ and the angle of dilation ψ are equal and the value of the meridional eccentricity ϵ is small. The use of the Mohr–Coulomb model involves asymmetric matrix storage and solution scheme in Abaqus/Standard because the plastic flow is usually non-associated. The parameters of the Mohr–Coulomb criterion can be determined using a triaxial compression symmetric laboratory test. For

cohesive soils, a minimum of two laboratory tests are required under different consolidation pressures to determine the parameters $\emptyset$ and c.

3.4.2. Drucker–Prager cap model

The Drucker-Prager cap model is suitable for simulating soil behaviour due to its ability to analyse the influence of stress history, stress path, dilatancy and the effect of the intermediate principal stress. Elastic behaviour can be modelled as linear elastic using the generalised Hooke's law. Alternatively, an elasticity model in which the bulk elastic stiffness K develops as the material experiences compression can be used to compute the elastic strains [28]. K is determined in accordance with Eq. 4:

$$K = \frac{(1 + e_0)\, p'}{\kappa} \tag{4}$$

where p' is the soil mean effective stress, e_0 is the soil initial void ratio and κ is the unloading−reloading line slope. Plastic behaviour can be modelled by determining the development of the failure surface and the cap yield surface as a function of stress invariants. The Drucker–Prager failure surface is given in Eq. 5:

$$F_s = t - p\, tan\, \emptyset - c = 0 \tag{5}$$

where $\emptyset$ is the slope of the linear yield surface in the *p–t* stress plane, which is the friction angle of the soil. The modified Drucker-Prager (MDP) cap model is a development of the Drucker-Prager plasticity model that includes a cap yield surface, thus providing an inelastic hardening mechanism to account for plastic compaction and helps to control volume dilatancy when the material yields in shear. The yield criteria for the modified Drucker–Prager cap model are based on the shape of the MDP cap failure surface in the meridional plane (*t–p*), which can have a linear, hyperbolic or general exponent form. The cap yield surface is an ellipse with eccentricity R, where its shape may be identified by t, which is found using Eq. 6. This equation depends on K_r, which is defined as the ratio of the yield stress in triaxial tension to the yield stress in triaxial compression. Thus, this value controls the dependence of the yield surface on the value of the intermediate principal stress, and the third invariant of deviatoric stress r.

$$t = \frac{q}{2}\left[1 + \frac{1}{K_r} - \left[1 - \frac{1}{K_r}\right]\left[\frac{r}{q}\right]^3\right] \tag{6}$$

The hardening or softening behaviour of the cap surface F_c is a volumetric plastic strain dependent. The cap yield surface F_c is given as follows, in Eq. 7:

$$F_c = \sqrt{(p - p_a)^2 + \left(\frac{R_t}{1+\alpha-(\alpha/\cos\emptyset)}\right)^2} - R(d + p_a \tan\emptyset) = 0, \tag{7}$$

where R is a material parameter that controls cap shape and α is a numeral parameter ranging between 0.01 and 0.05 which is utilised to define the smooth transition surface component F_t as given in Eq. 8:

$$F_t = \sqrt{(p - p_a)^2 + \left[t - \left(1 - \frac{\alpha}{\cos\emptyset}\right)(d + p_a \tan\emptyset)\right]^2} - \alpha(d + p_a \tan\emptyset) = 0, \tag{8}$$

In this expression, p_a is the evolution parameter which controls the hardening–softening behaviour as a function of the volumetric plastic strain. However, the hardening–softening behaviour is commonly defined by a piecewise linear function, which is associated with the mean yield effective stress p_b and the volumetric plastic strain (ε_{vol}^{Pl}), $p_b = p_b(\varepsilon_{vol}^{Pl})$. This relation can be obtained by the uniaxial isotropic consolidation test with several loading-unloading–reloading cycles.

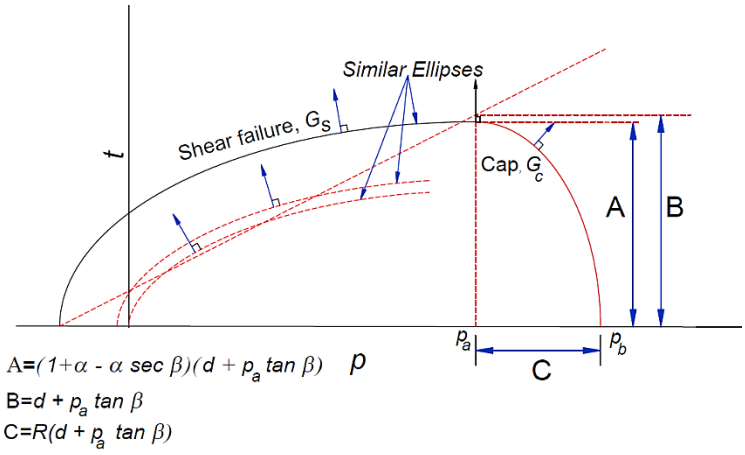

Figure 8. Flow potential of the modified cap model in the *p*–*t* plane.

$$G_c = \sqrt{(p - p_a)^2 + \left(\frac{R_t}{1 + \alpha - \alpha/\cos\beta}\right)^2} \tag{9}$$

$$G_s = \sqrt{[(p_a - p)\tan\beta]^2 \left(\frac{t}{1 + \alpha - \alpha/\cos\beta}\right)^2} \tag{10}$$

As shown in Fig.8, the potential plastic flow surface in the *p*–*t* plane comprises two segments. The cap region part is defined by a flow potential. Its associated flow yield surface is identical to its elliptical flow potential surface, as specified by Eq. 9. For the failure surface and the transition yield surface, the non-associated flow is assumed, and its potential flow surface expressed using Eq. 10.

The two elliptical components, G_c and G_s, produce a continued potential surface. The material stiffness matrix is not symmetric due to the availability of non-associated flow. Consequently, an asymmetric solver Abaqus option must be adopted in association with the cap model. For the material conditions in the current study, the linear model is adapted with non-associated flow in the *p*–*t* plane, presuming that the flow direction and yield surface are perpendicular in the $\prod$ plane and at the angle of ψ to the $t - axis$ in the *p*–*t* plane. Three triaxial compression tests are needed as a minimum requirement to compute the c and ϕ parameters. An isotropic consolidation test is needed to define the hardening–softening behaviour as a hydrostatic compression yield stress p_b and the corresponding volumetric plastic strain $\left(\varepsilon_{vol}^{Pl}\right)$ function [28]. The modified Drucker–Prager cap model may be used with plane strain, generalised plane strain, axisymmetric and 3D solid–continuum elements. However, it can never be used with elements in which the stress state is presumed as plane stress, such as shell and membrane elements [18].

3.4.3. Cam–clay model

The cam-clay and modified cam-clay (MCC) models were developed in the 1960's by researchers at Cambridge University [34] to describe the behaviour of soft soils. These models predict the pressure-dependent soil strength, compression and dilatancy caused by shearing, based on the philosophy of the critical state. On this basis, the models can forecast unlimited soil deformations without alterations in stresses or volume at the critical state. The MCC model adopts a fully saturated soil condition, and its formulations

are based on plasticity theory. It can define three significant aspects of soil behaviour, i.e. the soil strength, the volume change that occurs due to shearing, and the critical state which represents the location of unlimited distortion without any changes in stress or volume. However, as mentioned previously, in critical state mechanics, the state of a soil sample is characterised by three main parameters, i.e. the effective mean stress (p'), the shear stress q_{shear} and the specific volume V. The relationship between specific void ratio e and the natural logarithm of the mean effective stress $ln\, p'$consists of a straight virgin consolidation line, and a set of straight swelling lines, as shown in Fig. 9. The normal consolidation line (NCL) develops in the $e - p'$plane, and its equation in the $p' - q$ plane is $q = 0$.

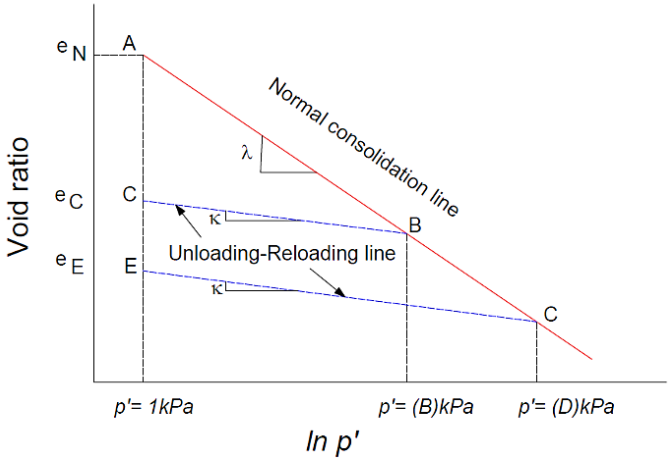

Figure 9. Consolidation Curve in the $e - lnp'$ plane

The values for $\lambda, \kappa, e_N\ and\ e_C$ as shown in Fig. 9 are the characteristic properties of a particular soil. Specifically, λ is the slope of the normal compression line, κ is the slope of the swelling line, e_N is the void ratio on the NCL at a unit mean effective stress and e_C varies for each swelling line and depends on the loading history of the soil. However, the critical-state line (CSL) is parallel to the NCL in the $e - lnp'$ plane, and its slope in the $p' - q$ plane, M which is the ratio of the shear stress, can be expressed in terms of internal friction angle $\emptyset'$ as follows:

$$M = \frac{6 \sin \emptyset'}{3 - \sin \emptyset'} \tag{11}$$

As shown in Figure 9, the shear stress at failure (shear strength) q_f is a function of the mean effective stress at failure p'_f. It is similar to the Mohr–Coulomb failure criterion, where c' is presumed zero for sands and soft clays. In other respects, the modified Cam–Clay yield surface is demonstrated in the $p' - q$ plane as an elliptical curve and can be expressed by Eq. 12:

$$\frac{q^2}{p'^2} + M^2 \left(1 - \frac{p'_c}{p'}\right) = 0 \tag{12}$$

In this expression, p'_c is the preconsolidation pressure which controls the size of the yield surface and varies in values for each unloading–reloading line. This parameter is utilised to define soil hardening behaviour. In geotechnical engineering, the elastic material properties usually used to define the stress−strain relationship are Young's modulus E, shear modulus G, Poisson's ratio υ and bulk modulus K. E and G are defined in Eqs. 13 and 14, respectively. In soil modelling, the shear modulus G and bulk modulus K parameters are employed to separate the influences of volume change and distortion on the behaviour. In MCC models, K is not constant, and is a function of p'.

$$E = 3K(1 - 2\upsilon) \tag{13}$$

$$G = \frac{3K\,(1-2v)}{2(1+v)} \tag{14}$$

For the isotropic, normally or lightly overconsolidated soil with an overconsolidation ratio (OCR) where $p'_C/p'_0 < 2$, and under drained conditions (soil specimen), the compression hardening behaviour is accomplished when the stress path touches the initial yield surface to the right maximum shear stress (q_f)−the wet side (see Fig. 10). The specimen experiences only elastic strains within the initial yield surface. Elastic and plastic strains are maintained when the stress state touches the yield surface, thereby promoting hardening and the further development of plastic strain until the stress state intersects with the CSL at point F, when failure occurs [28].

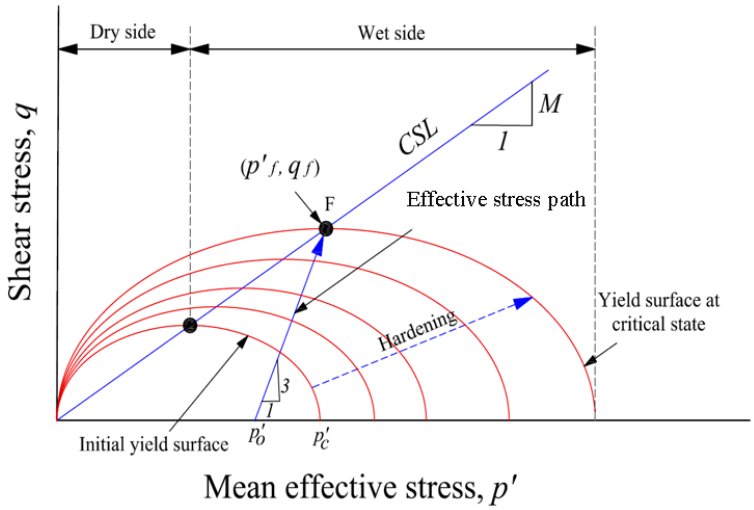

Figure 10. Cam–clay hardening behaviour including the evolution of the yield surface during hardening

For the isotropic, normally or lightly overconsolidated soil with $OCR = p'_C/p'_0 < 2$, and under drained conditions (soil specimen), the compression hardening behaviour is accomplished when the stress path touches the initial yield surface to the right maximum shear stress (q_f)−the wet side (see Fig. 10). The specimen experiences only elastic strains within the initial yield surface. Elastic and plastic strains are maintained when the stress state touches the yield surface, thereby promoting hardening and the further development of plastic strain until the stress state intersects with the CSL at point F, , when failure occurs [28]. However, the modified Cam–Clay model described earlier is a special case of the extended Cam–Clay model (ECC). The critical-state surface is presumed a cone in the space of principal effective stress. Its vertex concurs with the origin–zero effective stress, whereas its axis coincides with the hydrostatic pressure axis i.e., $\sigma'_1 = \sigma'_2 = \sigma'_3$. The conical critical-state surface projection on the $p-t$ plane is a straight line crossing through the origin with slope M. The plastic flow is presumed normal to the yield surface. The hardening rule controls the size of the yield surface, which has volumetric plastic strain dependence. The 3D yield surface is defined as follows Eq. 15:

$$f(p,q,r) = \frac{1}{\beta^2}\left(\frac{p}{a}-1\right)^2 + \left(\frac{t}{Ma}\right)^2 - 1 = 0, \tag{15}$$

where β is a constant used to modify the shape of the yield surface, and can be calibrated from a number of triaxial tests. It ranges between 0 and 1.0 [35], 0.787 was used in this study. α is the hardening parameter characterised, which defines the size of the yield surface, (t) is a shear stress measurement factor.

At least two laboratory experiments are needed to calibrate MCC model. An odometer test in addition to a one or more triaxial compression tests are essential to delivering a precise calibration. The onset of yielding

in the odometer test will directly give the initial location of the yield surface α_0. Before the logarithmic bulk modulus, κ and λ are also determined from pressure versus void ratio figure. For a valid model, $\lambda > \kappa$. The triaxial compression tests permit the calibration of the yield parameters $M$and β, [6]. The cam–clay model can be used in Abaqus with plane strain, generalised plane strain, axisymmetric and 3D solid elements. However, this model cannot be used with elements for which the supposed stress state is plane stress, such as shell and membrane elements. Table 4 represents the soil constitutive models' parameters corresponding to material properties of the soil used in numerical simulation.

Many parameters influence the cyclic behaviour of soft clay; (i) the level of cyclic stress which governs whether the soil can maintain a non-failure equilibrium state,[36];[37];[38];[39], (ii) cyclic loading frequency, which is liable for the rate of axial strains and the level of excess pore pressure, [40]; [41];[42]; [43];[44];[45]. (iii) OCR, which affects the effective stress paths and the degradation of the undrained shear modulus, [46];[47];[48]. (iv) and finally, the static pre-shearing factor that may decrease the cyclic shear strength thus improve the total shear strength, [49];[50];[51];[52];[53]. Carter et al. (1980,1982) [54] and [55] proposed a soil constitutive model based on MCC model, in which one additional parameter which defines the model cyclic behaviour is needed alongside with the parameters of MCC model. This parameter can be appropriately ascertained by employing the cyclic triaxial loading tests. However, the generation rate of excess pore pressures forecast based on this model increases lead to the ultimately soil failure. (Ni 2015) [56] proposed a new modification based on Carter et al. (1980, 1982), in which two additional cyclic degradation parameters are required to represent the yield surface function during elastic unloading. Cyclic stress ratio (CSR), pre-shearing, and cyclic loading frequency are considered in this model as well as in the current study.

The two additional parameters for the MCC model alongside with essential MCC soil properties and initial states parameters, are cyclic loading conditions including the values of cyclic degradation parameters $\xi_{d1}$and ξ_{d2} corresponding to specific CSR value, where $\xi_{d1}$and ξ_{d2} are experimental constants and related to the frequency of the applied cyclic loading see Table 4. The values of these two cyclic degradation parameters can be determined from undrained cyclic triaxial tests. $\xi_{d1}$and ξ_{d2} define the degree of the yield surface contraction once the soil is unloaded elastically, and consequently the level of excess pore pressures and axial strains parameters are generated for each cycle. These two parameters are a function of the period of each cycle. User-defined Material UMAT - Fortran subroutine has been linked in Abaqus in order to consider the two aforementioned cyclic degradation parameters $\xi_{d1}$and ξ_{d2} to MCC model. However, as the current study provides a guideline to the researcher for transferring the physical tests to the numerical simulation, the researcher may choose a more appropriate soil model to represent their dynamic problem. Three examples of advanced cyclic soil models, i.e., bounding surface plasticity model [57];[58], multi-surface plasticity model [59];[60]could be an excellent solution depending on the nature and complexity of the problem.

Table 4 Model parameters for the soil constitutive models

Parameter	**Value**
Density, (kg/m^3)	1505.75
Log Bulk Modulus	0.05
Poisson's Ratio	0.47
Tensile Limit (MPa)	0.00
Log Plasticity Bulk Modulus	0.27
Stress Ratio	1.26
Wet Yield Surface Size	1.00
Flow Stress Ratio	0.78
Angle of friction (Degrees)	10.00

Cap Eccentricity			0.90
Transition surface radius (m)			0.04
Initial Void Ratio			1.50
Cyclic loading parameters			
Freq. (Hz)	CSR	ξ_{d1}	ξ_{d2}
0.1	0.6	4.2	75
0.25	0.6	4.2	97
1	0.6	4.1	420
2	0.6	4.1	600
5	0.6	4.2	825
10	0.6	4.2	1065

4. Validation of the numerical model

In this section, the finite element model developed in the previous section is employed to simulate the physical shaking table experiments discussed previously, namely tests 1.15 and 2.26 from phase II of the PEER Centre test programme [17], to validate the numerical approach. In the first instance, the three different soil constitutive models are examined, denoted as the MC (Mohr-Coulomb), DP (Drucker-Prager) and CC (cam–clay) models, respectively, to determine which is the most appropriate for this type of problem. The FE simulation consists of four single piles with head masses varying from 4.5 kg to 72.7 kg embedded in 2.0 m of soil deposit. As in the reference case study, the model was subjected to a series of scaled seismic excitation, such as the YBI90, which is the input motion for Test 1.15, and the KPI79N00, which represents the test 2.26 loading. The results are assessed in terms of acceleration time histories, fast Fourier transforms (FFTs) and 5% damped response spectra. In addition, bending moment envelopes were calculated at the nodes located in the same position as the physical model pile strain gauges in the shaking table tests, to enable a comparison of this data.

4.1. Simulation of the free-field response

In an SSPSI analysis, one of the most critical factors is achieving an accurate depiction of the free-field site response as any error in this calculation can directly propagate into and intensify during the soil–pile analysis. To evaluate the dynamic soil–structure interaction problem correctly, the free-field responses of the numerical simulation of the three soil constitutive models were compared. These responses were represented as the soil accelerations recorded at different levels along the soil column depth, with the physical shaking table response. Finally, the results were validated with those numerically simulated using the ground response analysis software SHAKE91, which is designed to performing an equivalent linear seismic response analyses of a horizontally layered soil [61]. The model container for the physical and numerical tests in addition to the distribution of soil displacements are shown during strong shaking in Fig. 11. Modulus degradation, damping curves and shear wave velocity are the main soil model parameters required to be employed in Shake91 software. The values for degradation of soil modulus and damping recommended by Sun et al. [62] and Dobry [63] for Young Bay mud cohesive soils are employed as the input parameters in the numerical analysis, in addition to a test-specific shear wave velocity profile. Consolidation and triaxial tests that are provided in the reference study were used to produce the essential soil properties for the FE model.

A series of SHAKE91 trial simulations was performed in the reference case study to examine the model performance following several parametric studies, i.e., the shear wave velocity profile and the modulus degradation and damping curves. Indeed, these tests confirmed the strong sensitivity of the results to variations in the shear wave velocity profile and the modulus degradation and damping curves. Based on the

analysis of other researchers [e.g.32] it was found that enlarging the shear wave velocity values by 30% from the test-specific stiffness profiles provided optimal results and therefore this strategy is also adopted in the current work.

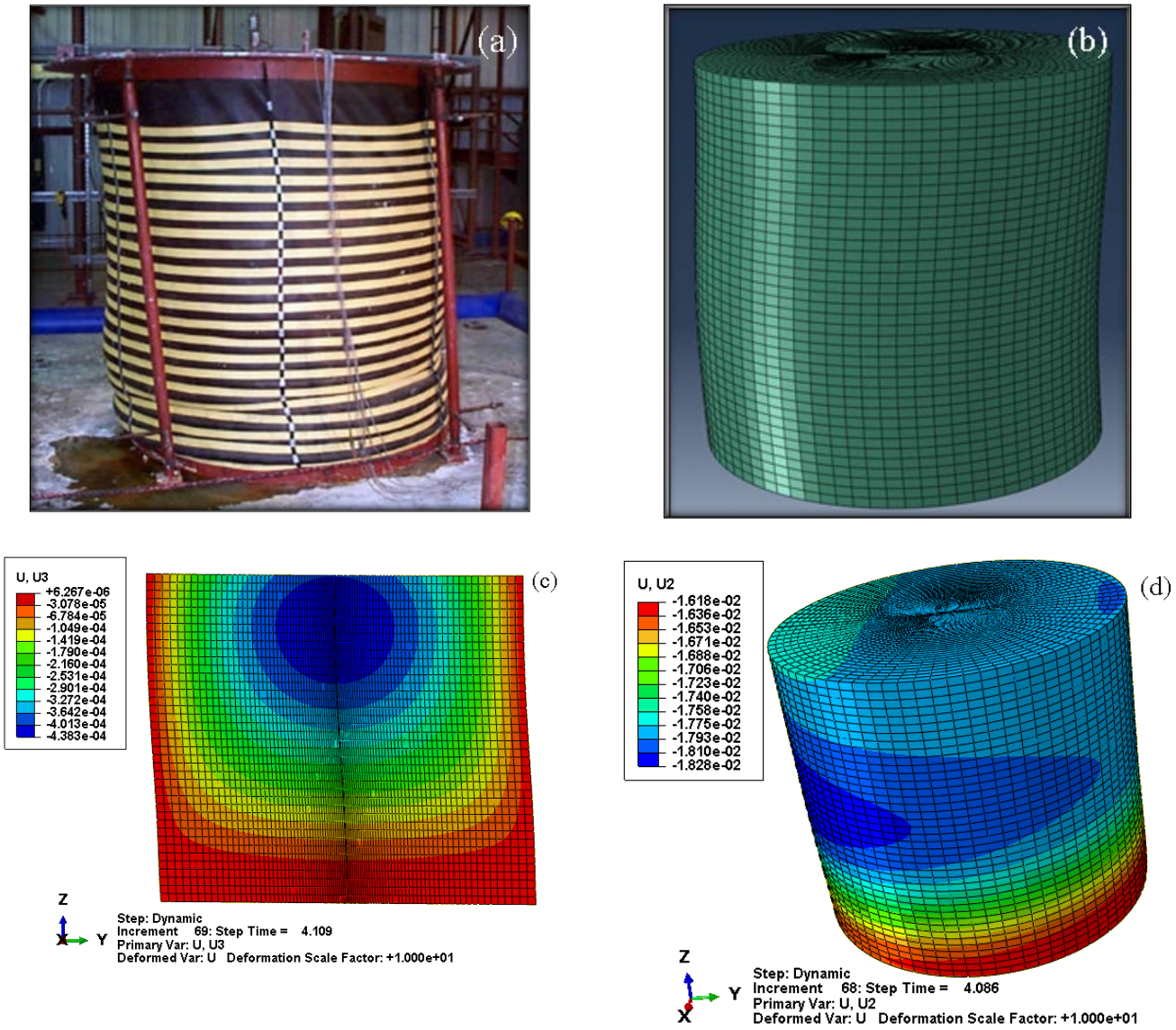

Figure 11. Physical and numerical model soil container in motion during strong shaking, including (a) the physical soil container in motion [4], (b) the numerical model soil container in motion, (c) the distribution of soil displacement in motion, and (d) the distribution of soil displacement in motion

Fig. 12 presents the results of the spectral acceleration response along eight elevations of the soil deposit depth for the free field analysis case for Test 2.26. To ensure that the accelerations in the soil response are accurately predicted, these results have been selected at the model elements in accordance with the accelerometer positions during the physical test. Depending on the applied soil constitutive model, four different levels of accuracy (Accuracy of being close to physical test findings) have been achieved, ranging from the best to worst accuracy for CC, DP, SHAKE91, and MC model respectively.

Based on the results presented in Fig. 12, it is concluded that the numerical simulation model is successful in depicting the free field case. The model boundary conditions are sufficiently restrained from simulating the free field conditions in the soil effectively, and therefore this aspect of the numerical modelling is validated. The predicted values of the peak ground acceleration (PGA) obtained by SHAKE91 at the soil surface is slightly lower than that from the physical test. On the other hand, the MC model tends to over-

predict the PGA whilst the DP model provides an acceptable PGA predicted value which has a small deviation to physical test value. The CC model produces the most accurate depiction of the true behaviour.

Moreover, the spectral acceleration response accomplished in physical test at the predominant input motion periods of 0.12 sec, is 0.35 (g). The CC model precisely predicts these values, and lesser degrees of accuracy are achieved for the SHAKE91, DP and MC models. In conclusion, both the CC finite element model and the SHAKE91 approach provide an accurate depiction of the physical model soil response in two different scale levels of precision. The numerical model of the soil-container system can replicate the free-field site response accomplished by physical test adequately.

There are some small deviations between the results from the physical test and numerical model but these are considered to be in the acceptable range as there is only one material dependence model (only soil model has been simulated), i.e. kinematic interaction function response. However, the propagation of these errors into the complete soil-pile structure interaction analysis requires careful consideration and the selection of an appropriate soil constitutive model and precise scaling methodology are critical.

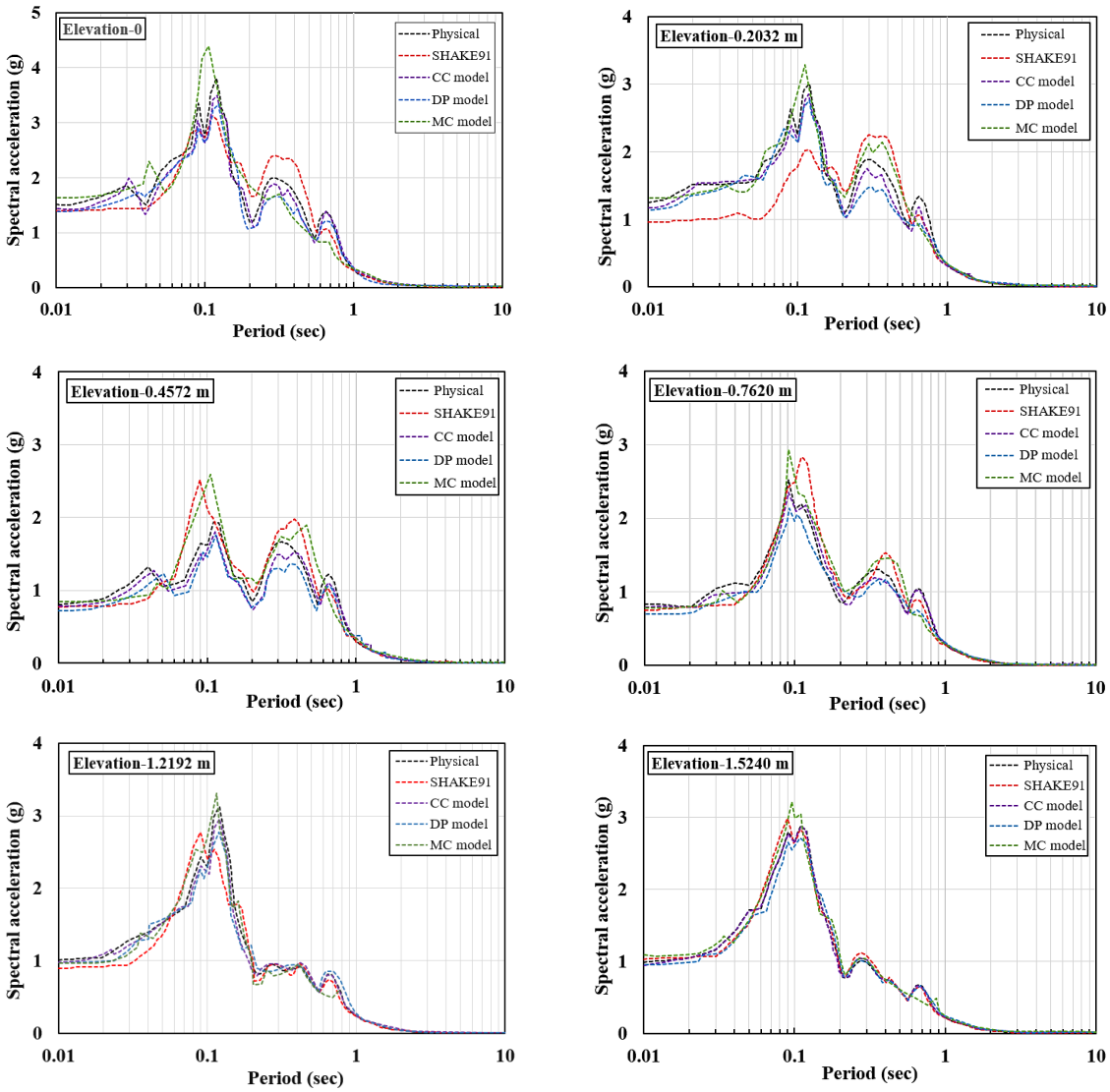

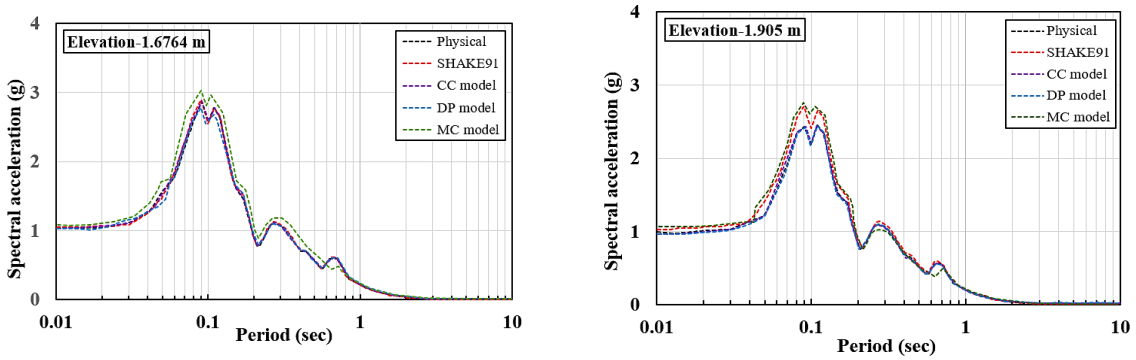

Figure 12. Numerical predictions for the behaviour of physical Test 2.26 in terms of acceleration response spectra (elevations are in m, relative to top surface)

4.2 Kinematic versus inertial pile response

As previously identified, SSPSI response modes comprise components of the superstructure inertial forces and also the kinematic forces exerted by the soil on the pile. Decoupling these variables and analysing the inertial and kinematic interaction independently for their corresponding contributions to SSPSI is important to understand the individual effects. However, the crucial issue is that the relative proportions of inertial and kinematic interaction are magnitude dependent. Therefore, determining these components from the physical or numerical model and then examining the decoupling assumptions provides an effective approach. However, physical and numerical dynamic simulation for single piles offers the best opportunity for isolating these mechanisms of SSI. A strong relationship between SSPSI and the pile response was reported in the case study [17], and this relationship has also been captured in numerical analysis with different degrees of accuracy depending on the type of soil constitutive model. Fig. 13 illustrates four examples of the numerical simulation model response for Test 1.15 for the four loading cases in the relevant directions.

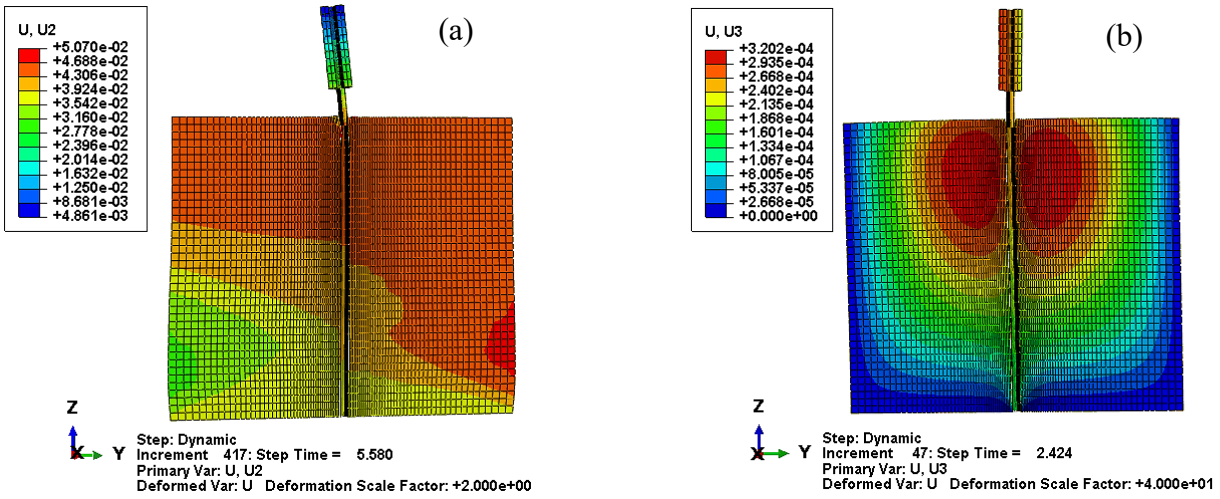

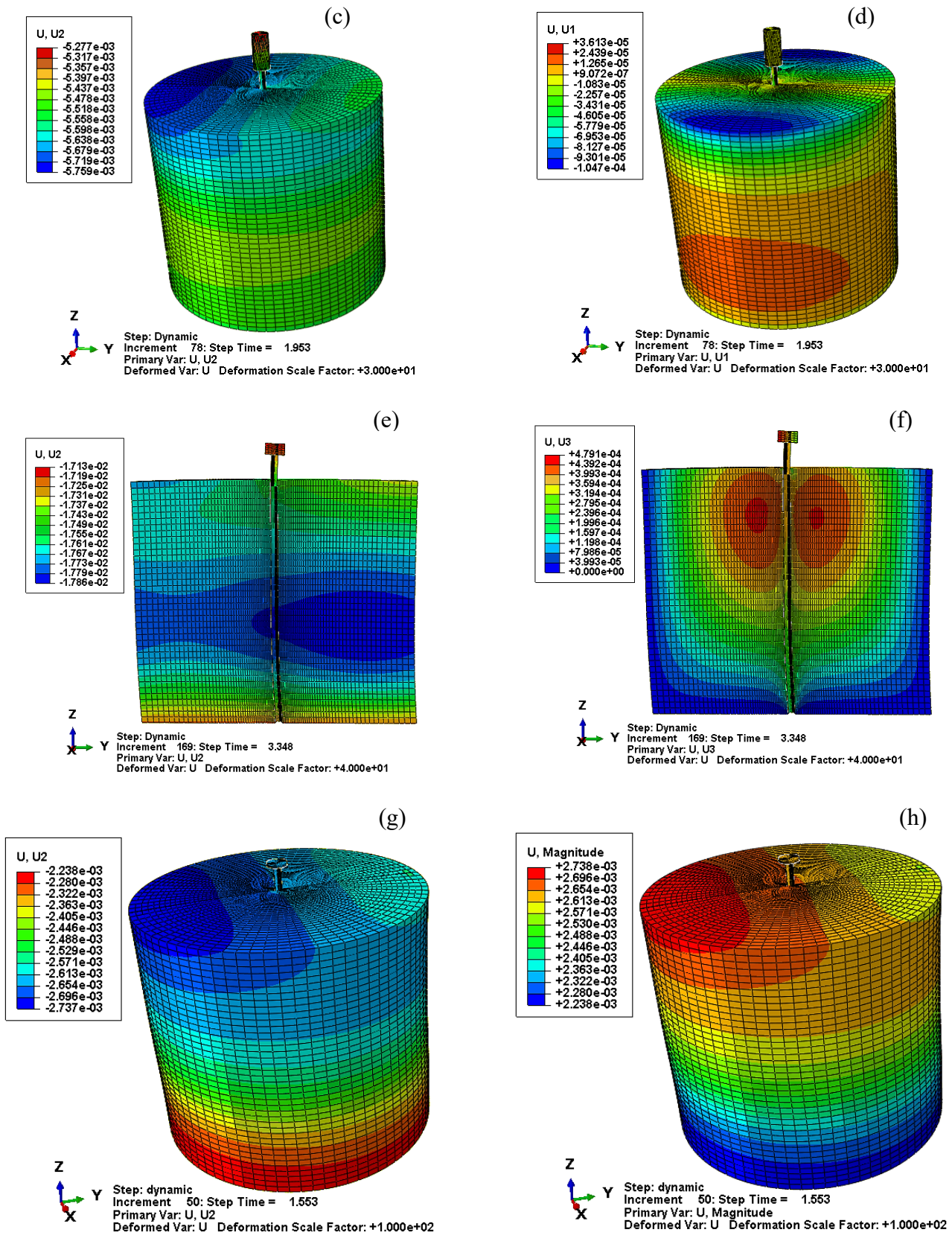

Figure 13. Numerical simulation model response for Test 1.15 showing the displacements in (a) the y-direction for the 72.7 kg pile head case, (b) the z-direction for the 72.7 kg pile head case, (c) the y-direction for the 45.3 kg pile head case, (d) the x-direction for the 45.3 kg pile head case, (e) the y-direction for the 11.4 kg pile head case, (f) the z-direction for the 11.4 kg pile head case, (g) the y-direction for the 3.0 kg pile head case, and (h) the magnitude displacement for the 3.0 kg pile head case

In the reference case study, the bending moment envelopes for the four piles were computed and plotted from the model pile strain gauges located at specific locations [17]. Accordingly, in the numerical simulation, the bending moment envelopes are described by the absolute maximum bending moment at the points which are corresponding to the location of the strain gauges in the physical test during the excitation. It is not equivalent to the actual bending moment diagram at the time step.

Fig. 14 and Fig. 15 present the experimental and numerical data of the bending moment envelopes for the four head pile cases. The comparison of the two set of results reveals that the interaction mode of the inertial forces which develop due to the effects of the superstructure (pile head masses) dominate the heavily loaded pile response. This inertial interaction induces a significant bending moment at the vicinity of the pile heads. The interaction of kinematic forces significantly influences the lightly loaded piles and induces maximum bending moments at a depth of 0.762 and 0.762 m, respectively. The differences between the physical test results and the numerical simulation are relatively small indicating the following: (i) the FE simulation of the physical shaking table test is performed successfully, (ii) both inertial and kinematic interaction of the SSPSI system can be captured accurately, and (iii) using an effective soil constitutive model and appropriate numerical modelling aspects (constraint, contact, loading and boundary conditions) are the key of achieving accurate results.

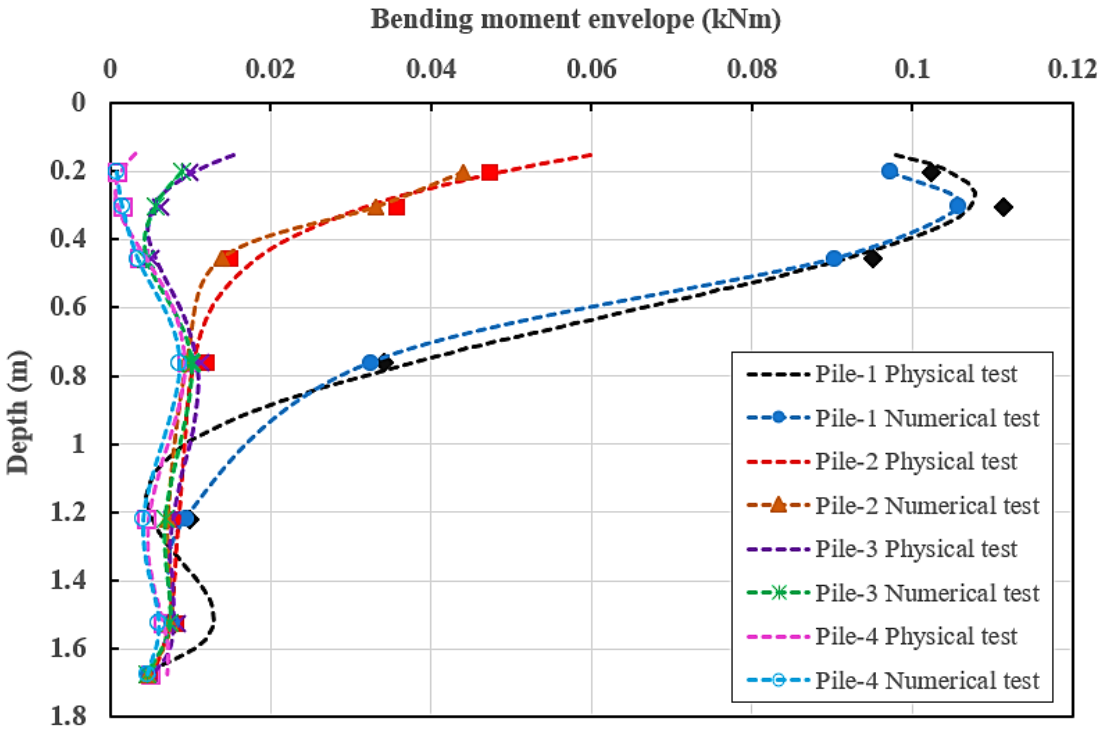

Figure 14. Comparison of the experimental and numerical pile bending moment envelopes for Test 1.15, using the CC soil model, for piles with a mass head of 72.7 kg (Pile-1), 45.4 kg (Pile-2), 11.4 kg (Pile-3) and 3.0 kg (Pile-4)

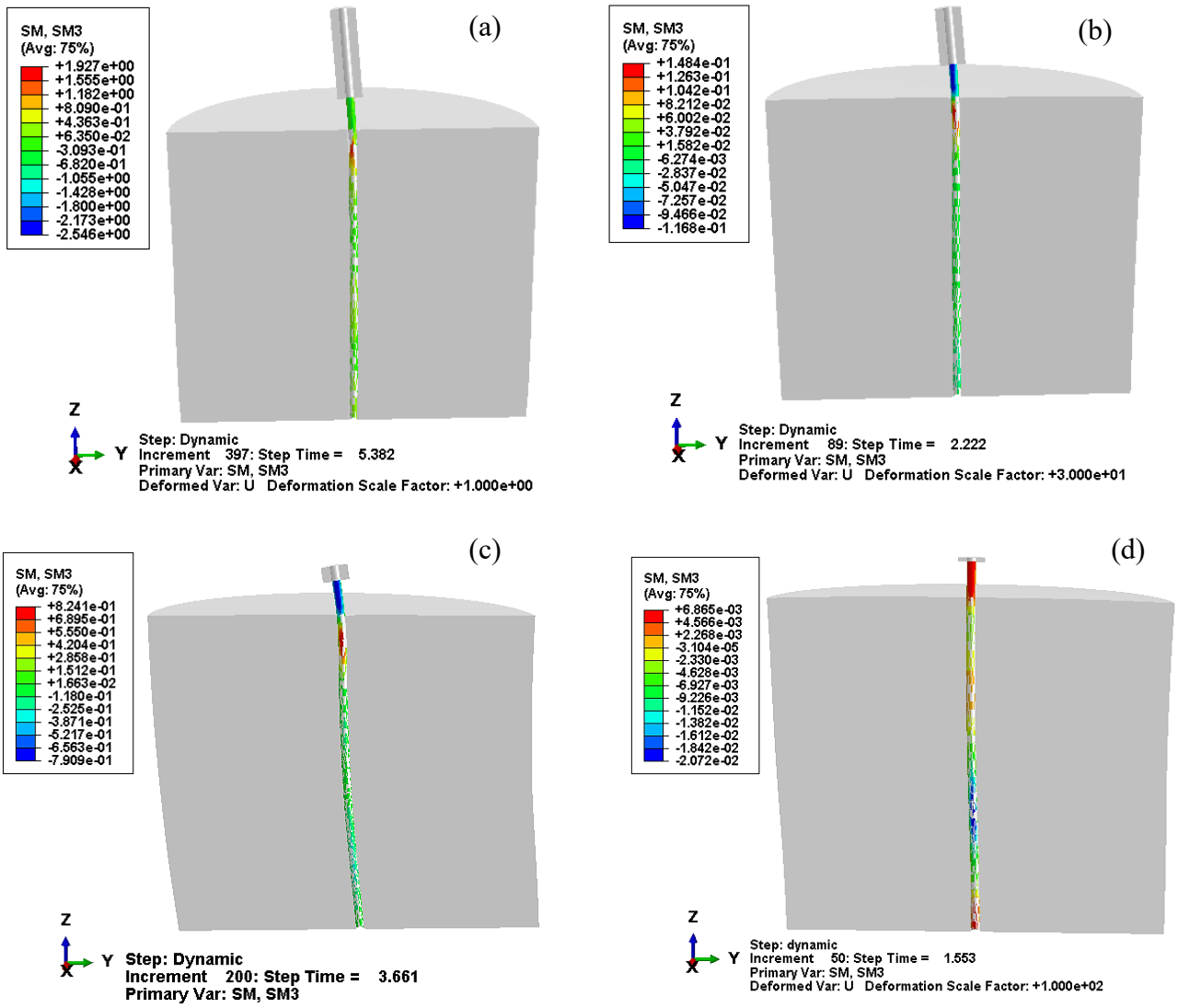

Figure 15. Pile bending moments along the z-axis for Test 1.15 during shaking for a pile with a mass head of (a) 72.7 kg (Pile-1), (b) 45.4 kg (Pile-2), (c) 11.4 kg (Pile-3) and (d) 3.0 kg (Pile-4)

Fig. 16 presents (a) the pile head accelerations and (b) the fast Fourier transforms (FFTs) for a single pile model with a head weight equal to 72.7, 45.4, 11.4 and 3.0 kg, respectively for Test 1.15 [4]. Three different soil constitutive models are included in the images, as well as the physical test data. Although the structure and soil deposit interact with the foundation system and may behave in the plastic range under specific earthquakes, most studies focus on the elastic response system to simplify the problem, especially for soil material. The results when the MC model is employed, as shown in Fig. 16, indicate that significant errors in the SSPSI system behaviour develop during seismic loading. There are a number of explanations for these errors, which are outlined as:

1. The MC soil constitutive model is most appropriate for monotonic loading conditions, rather than during seismic events,
2. The MC model is more appropriate for simulating less soft clays subjected to monotonic loading. Therefore, when the soil is shearing beyond the elastic limit (into the plastic range), the model tends to overestimate the effective stress values. This is indicated clearly in Fig.16, through the significant jump in Fourier amplitude values in the values obtained using the MC model.

3. The stress and stress-path dependency of the soil stiffness are not incorporated in the MC model, and the model does not include the strength reduction component, which is essential for simulating cyclic behaviour [64].

A number of previous studies have revealed that using the MC model provides reasonable results, but the analyses were performed within the small-strain range and monotonic loading conditions and therefore do not capture the issues with seismic conditions [5]. The results presented in Fig.16 also indicate that although these errors exist to some extent when the Drucker–Prager model is used, the errors are smaller than for the MC soil model.

In accordance with the reference case study, the piles with larger head masses experience more significant bending moments at the pile head, leading to high plastic strains in this region. Consequently, damping increases dramatically, contributing to a significant reduction in the acceleration amplitude of the pile head. This phenomenon may justify the greater divergence between the simulation results and those from the physical test simulated using MC and DP models, as the inertial force increases significantly due to seismic excitation effect.

The gap-slap mechanism is employed in this simulation. The gap evolution develops in the unconfined space along the pile length. Consequently, the pile has a large space to move horizontally, and then free vibration can occur. Permanent gap deformity is monitored after the shaking phase with the values matching those that occurred the reference physical case study. However, the comparison of the size of the generated soil-pile gap values with those from the reference case study depends largely on the type of the modelling criteria and the best results were provided by the CC model, followed by the DP model and then the MC simulation. Similar to the physical shaking table results, the piles with relatively higher mass heads develop greater gap-slap mechanisms. By contrast, the influence of the soil kinematic force dominates the piles with relatively lower head mass. Once the gap between the soil and pile develops, the friction resistance of the pile skin reduces as does the pile capacity, and more space develops between the two components allowing for pile free vibration. This is mainly relevant for pile systems with high head masses.

From the results presented in this paper, it is observed that nonlinear numerical analyses are a practical and useful way of simulating the SSPSI problem, although the accuracy is very dependent on the selection of a suitable soil constitutive model. For a dynamic soil-structure interaction analysis, as presented herein, the cam-clay (CC) model is considered to give the best results. Furthermore, the small deviation between the physical and numerical results when the CC model is employed may reflect the conditions of constructing the physical shaking structure, which include a close proximity between the accelerometer array to the adjacent part of the shaking table and other model structures, which in turn added to the feedback energy that arises from those members and being recorded by the accelerometers. This phenomenon has been observed in several field case studies presented in the literature [65]. Moreover, the strong twist motions provided by the shaking table, which cannot be isolated from the test data and are difficult to consider in the numerical analyses, may represent another possible justification for the under-prediction of behaviour from the CC model.

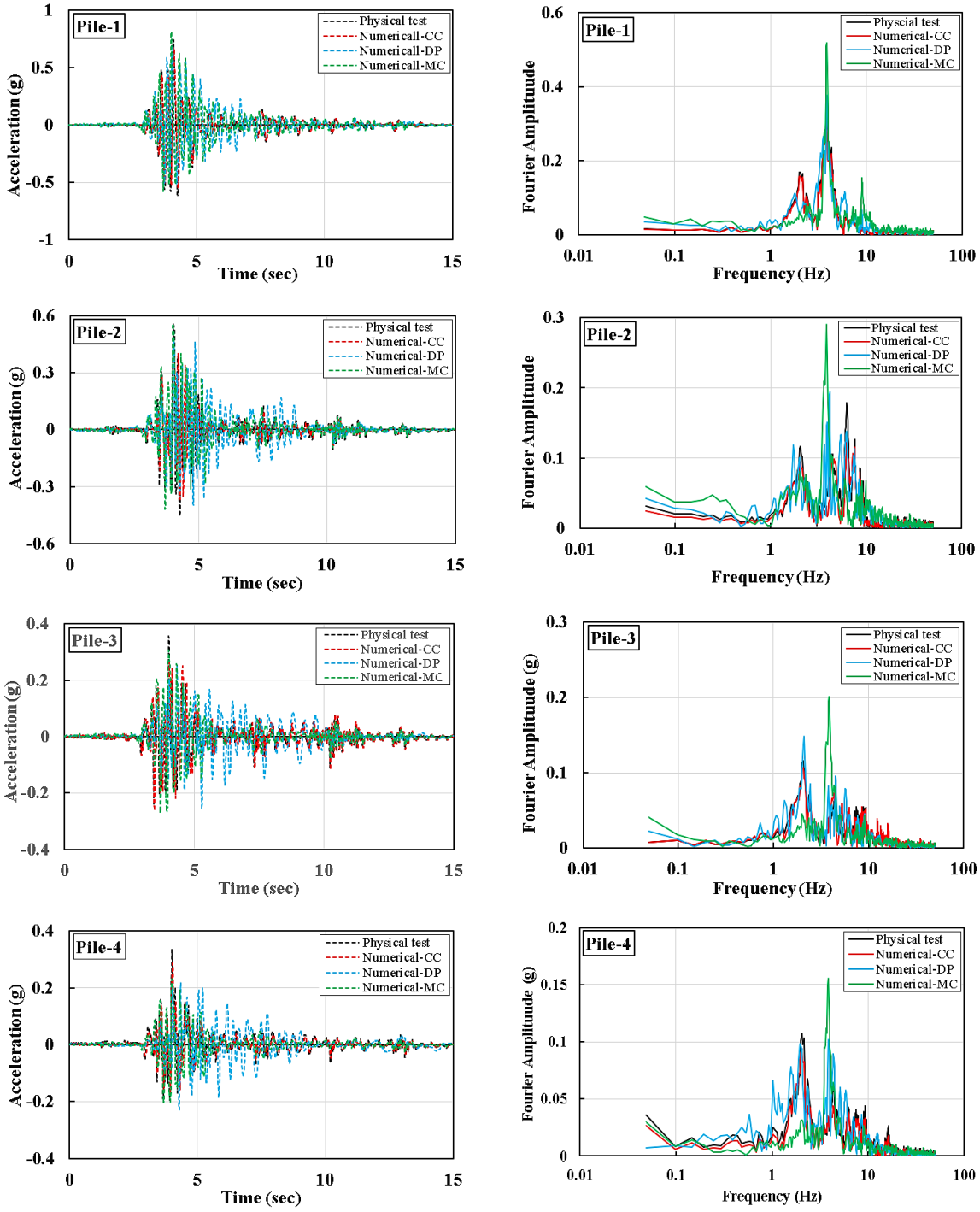

Figure 16 Physical test versus numerical simulation showing (a) pile head acceleration time histories and (b) fast Fourier transforms (FFTs) for the four piles under examination

A qualitative comparison between the resultant motion properties for both the physical and numerical tests are given in Table 5, which represent the values of the motion parameters such as maximum acceleration (g), time of maximum acceleration (sec), predominant period (sec), number of effective cycles, sustained maximum acceleration (g) and effective design acceleration (g). Vibration period is an essential factor in base-shear design methodology, and is a critical parameter in defining the design response spectrum and consequently controlling the value of the base shear force. It is observed in Table 5 that the predominant periods and number of effective cycles from the numerical analysis for all four pile head masses is quite similar to the equivalent values from the physical test when the cam-clay soil constitutive model is used.

Table 5 The resultant motion properties for both physical and numerical tests

Parameters	Pile-1				Pile-2				Pile-3				Pile-4			
	Test	Numerical simulation			Test	Numerical simulation			Test	Numerical simulation			Test	Numerical simulation		
		CC	DP	MC		CC	DP	MC		CC	DP	MC		CC	DP	MC
Max. Acc. (g)	0.745	0.74	0.689	0.812	0.534	0.438	0.477	0.560	0.356	0.305	0.256	0.307	0.333	0.287	0.230	0.231
Time of Max. Acc. (sec)	4.09	4.1	4.06	4.03	4.03	4.03	4.04	4.0	4.02	4.03	5.29	4.07	4.0	4.03	4.29	4.05
Predominant Period (sec)	0.24	0.24	0.25	0.27	0.15	0.14	0.16	0.26	0.23	0.24	0.2	0.26	0.22	0.22	0.2	0.26
No. of Effective Cycles	1.359	1.359	2.690	1.727	2.030	2.137	3.730	2.106	1.978	1.776	4.214	3.126	1.461	1.417	4.006	2.410
Sustained Max. Acc. (g)	0.370	0.365	0.576	0.578	0.304	0.256	0.363	0.407	0.198	0.236	0.206	0.258	0.141	0.154	0.202	0.196
Effective Design Acc. (g)	0.767	0.707	0.636	0.845	0.558	0.532	0.482	0.572	0.358	0.335	0.254	0.378	0.336	0.286	0.231	0.268

In order to examine the nonlinear behaviour of the system, the dynamic *p-y* curves are developed. In pile design, the soil is represented by a series of nonlinear *p-y* curves which vary according to depth and soil type; therefore in the current study, four specific points (at 2d, 4d, 6d, and 8d, where d is the pile's diameter) are selected to represent different points along the pile length, where *p* is the soil pressure per unit length of the pile and *y* is the pile displacement. The *p-y* curve methodology has been successfully executed for the seismic test data, during test 1.15. However, it is valuable to extract a section of the *p-y* time history for the loading range of interest. Thus, Figure 17 illustrates the time window of the *p-y* analysis in terms of the *p* time history (*p* in MPa). Figure 18 presents the *p-y* curves at the depths of (a) 2d, (b) 4d, (c) 6d and (d) 8d for Pile 1 of Test 1.15, assuming a head mass of 72.4 kg to effectively mobilize *p-y* resistance. The dynamic *p-y* resistances are compared with the API cyclic curves proposed by Meymand (1998). It is shown that the *p-y* curves match the API cyclic curves very well, both in terms of initial stiffness and ultimate strength. There is a clear demonstration of both hysteretic and degrading behaviour, particularly at depths of 4d and 6d. The low stiffness detected at 4d and 6d illustrates that the pile is crossing the gap previously opened during Test 1.15, thus indicating that gapping is a critical feature to include in the analytical model. These findings also serve as a back-analysis validation of using *p-y* curves for SSPSI problems. The effective stress rate $\dot{\sigma}'$ is a tensor valued function of the rate of strain $\dot{\varepsilon}$, effective stress σ' , void ratio e, intergranular strain tensor δ and a non- linear viscous strain rate tensor $\dot{\varepsilon}_v$ as an additional variable:

$$\dot{\sigma}' = H(\sigma', e, \delta, \dot{\varepsilon}, \dot{\varepsilon}_v) \tag{16}$$

For MCC model viscous effects is appropriate for the OCR is less than 1.4–viscous effects raise with a viscosity index Iv that ranges between 0.02 to 0.06 for hard and soft clay. However, for OCR greater than 1.4 the hypoplastic response is relevant [66].

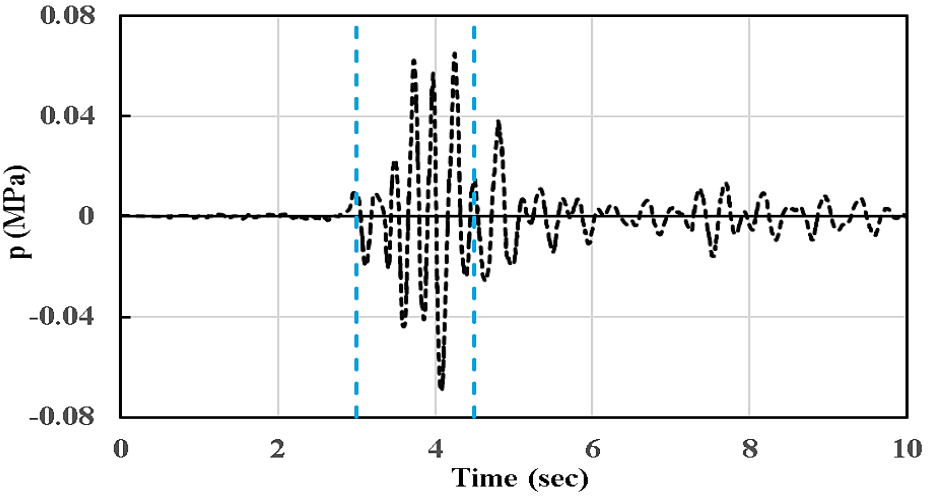

Figure 17 Time window for the *p-y* curve for Pile 1 of Test 1.15

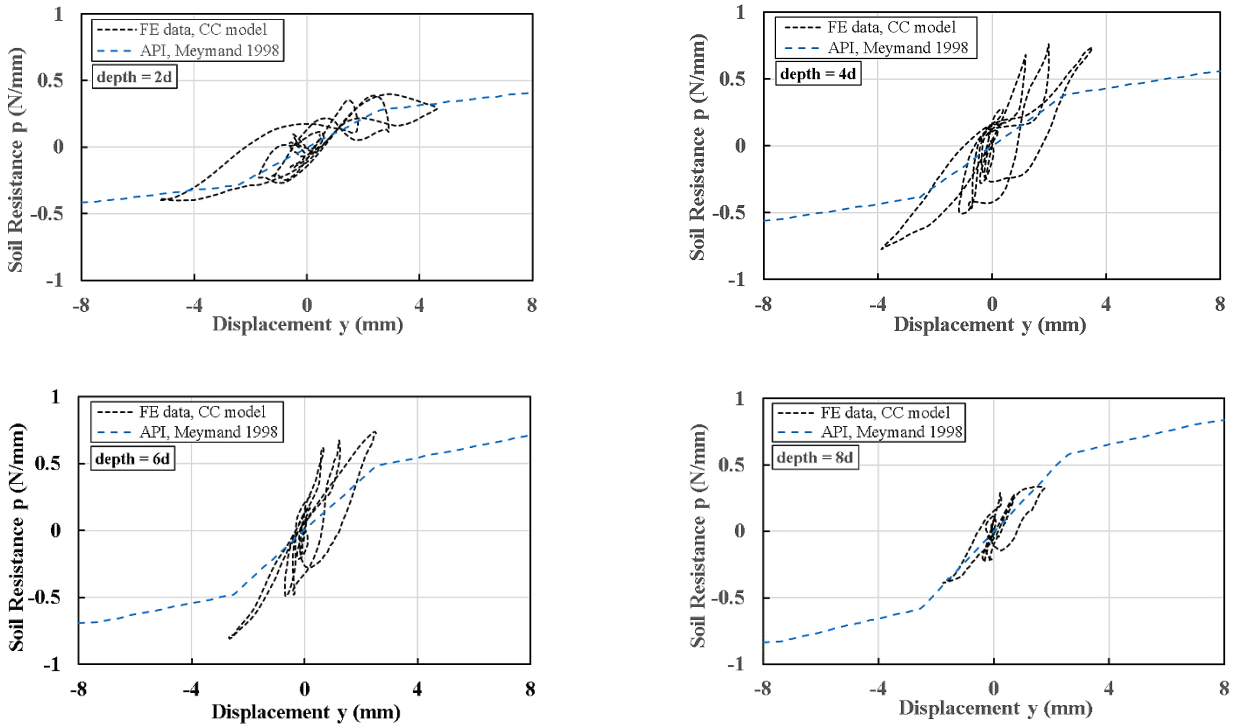

Figure 18 *p-y* curves for Pile-1 of Test 1.15 at depths of (a) 2d, (b) 4d, (c) 6d and (d) 8d

5. Concluding remarks

This paper has described the development of a numerical model which can accurately depict seismic soil–pile–superstructure interaction (SSPSI) problems. This is a very challenging problem, but essential in order to develop a greater understanding of this behaviour for real structures. The novelty of this work is in the development of a fully coupled nonlinear seismic soil-structure interaction numerical model for a scaled shaking table test. This includes both material and geometric nonlinearities for both the soil and pile behaviour, and three elastoplastic soil constitutive models were analysed.

The research presented herein has largely focused on the influence of the soil constitutive model, and three different models have been examined. The dimensional analysis procedure to determine appropriate scaling criteria to develop a scaled soil and pile-supported structure in the model, is described. A unique methodology is outlined which allows multi-directional simple shear deformations, minimises boundary effects and replicates the free-field site response. The output data from the model is validated using available physical test data and it is shown that the model provides an accurate representation of the test behaviour.

The finite element analysis software Abaqus is employed to develop a 3D numerical model to replicate a physical shaking table test. Three different soil constitutive models are examined including the Mohr–Coulomb model, the Drucker–Prager cap model and the Cam–Clay model. It is shown that using an appropriate soil constitutive model is key to providing an accurate representation of the physical test. The dynamic pile response is also studied, and a fully-coupled analysis procedure is developed which can accurately represent the dynamic response of complex soil–pile–superstructure systems.

The majority of soil–structure interaction effects such as the gap-slap mechanism, the consequences of the soil-pile kinematic force, and the superstructure inertial force, are clearly shown and depicted in the model. The consequences of SSPSI illustrates that the gap-slap mechanism amplifies the pile head acceleration, lengthens the period of the superstructure and activates the pile free vibration, thereby leading to a reduction in stiffness of the pile. Therefore, ignoring the gap-slap mechanism due to simplification of numerical analysis results in misleading stiffness and strength capacity of the analysed piles. It is important that this

is included in the numerical model. Although there are some small differences between the numerical results and those from the physical tests, these are within an acceptable range and the physical shaking table test is successfully simulated using FEA, particularly when the cam-clay soil model is employed. The Mohr–Coulomb and Drucker–Prager cap models provide a less accurate representation of the considered problem and are generally shown to be unsuitable for non-monotonic loading conditions.

References

[1] A. Emadi, H. Shakib, and M. Shadlou, "Investigation of beneficial and detrimental effects of soil-foundation-structure interaction on the seismic response of shear buildings," *KSCE J. Civ. Eng.*, vol. 18, no. 1, pp. 253–263, 2014, doi: 10.1007/s12205-014-0202-2.

[2] B. K. Fan, G. Gazetas, A. Kaynia, E. Kausel, and S. Ahmad, "Kinematic seismic response of single piles," *J. Geotech. Eng.*, vol. 117, no. 12, pp. 1860–1879, 1992.

[3] W. C. Stone and F. Y. Yokel, "Engineering Aspects of the September 19, 1985 Mexico Earthquake," Washington, D.C., 1987.

[4] R. M. Varghese and G. Madhavi Latha, "Shaking table tests to investigate the influence of various factors on the liquefaction resistance of sands," *Nat. Hazards*, vol. 73, no. 3, pp. 1337–1351, 2014, doi: 10.1007/s11069-014-1142-3.

[5] V. S. Phanikanth, D. Choudhury, and G. R. Reddy, "Behavior of Single Pile in Liquefied Deposits during Earthquakes," *Int. J. Geomech.*, vol. 13, no. 4, pp. 454–462, 2013, doi: 10.1061/(asce)gm.1943-5622.0000224.

[6] N. Stromblad, "Modeling of Soil and Structure Interaction Subsea," Chalmers University of Technology,Sweden, 2014.

[7] T. Tipsunavee and G. Arangjelovski, "Three Dimensional Analysis of Soil-Pile-Structure Interaction Problem in Soft Clay Simulation of Shaking Table Test," 2015, no. July, pp. 1–6.

[8] P. J. Meymand, M. F. Riemer, and R. B. Seed, "Large scale shaking table tests of seismic soil-pile interaction in soft clay," in *12th World Conference on Earthquake Engineering*, 2000, p. 2817.

[9] M. G. Durante, L. Di Sarno, G. Mylonakis, C. A. Taylor, and A. L. Simonelli, "Soil–pile–structure interaction: experimental outcomes from shaking table tests," *Earthq. Eng. Struct. Dyn.*, vol. 45, no. 7, pp. 1041–1061, 2016.

[10] S. Brown, "Copyright - 2007," no. May, pp. ii–ii, 2011, doi: 10.1109/wons.2007.340472.

[11] S. Li, F. Zhang, J. Wang, M. S. Alam, and J. Zhang, "Seismic responses of super-span cable-stayed bridges induced by ground motions in di ff erent sites relative to fault rupture considering soil-structure interaction," *Soil Dyn. Earthq. Eng.*, vol. 101, no. September 2016, pp. 295–310, 2017, doi: 10.1016/j.soildyn.2017.07.016.

[12] J. Yang, P. Li, and Z. Lu, "Large-scale shaking table test on pile-soil-structure interaction on soft soils," *Struct. Des. Tall Spec. Build.*, vol. 28, no. 18, pp. 1–19, 2019, doi: 10.1002/tal.1679.

[13] Z. Chen, P. Yang, H. Liu, W. Zhang, and C. Wu, "Characteristics analysis of granular landslide using shaking table model test," *Soil Dyn. Earthq. Eng.*, vol. 126, no. July, p. 105761, 2019, doi: 10.1016/j.soildyn.2019.105761.

[14] W. Zhang *et al.*, "Study on seismic behaviors of a double box utility tunnel with joint connections using shaking table model tests," *Soil Dyn. Earthq. Eng.*, vol. 136, no. May, p. 106118, 2020, doi: 10.1016/j.soildyn.2020.106118.

[15] M. P. Romo, M. J. Mendoza, and S. R. García, "Geotechnical factors in seismic design of foundations state-of-the-art report," *Bull. New Zeal. Soc. Earthq. Eng.*, vol. 33, no. 3, pp. 347–370, 2000.

[16] Y. Khodair and A. Abdel-Mohti, "Numerical Analysis of Pile–Soil Interaction under Axial and Lateral Loads," *Int. J. Concr. Struct. Mater.*, vol. 8, no. 3, pp. 239–249, 2014, doi: 10.1007/s40069-014-0075-2.

[17] P. J. Meymand, "Shaking table scale model tests of nonlinear soil-pile-superstructure interaction in soft clay," 1998.

[18] M. Smith, "ABAQUS/Standard User's Manual, Version 2018." Dassault Systèmes Simulia Corp, Providence, RI, p. 1146, 2018.

[19] A. T. Al-Isawi, P. E. F. Collins, and K. A. Cashell, "Fully Non-Linear Numerical Simulation of a Shaking Table Test of Dynamic Soil-Pile-Structure Interactions in Soft Clay Using ABAQUS," *Geotech. Spec. Publ.*, vol. 2019-March, no. GSP 308, pp. 252–265, 2019, doi: 10.1061/9780784482100.026.

[20] S. J. Kline, *Similitude and Approximation Theory*. Stanford,U.S.A: Springer-Verlag, Berlin Heidelberg New York Tokyo, 1986.

[21] P. D. Moncarz and H. Krawinkler, *Theory and Application of Expermental Model Ananlysis in Earthquake Engineering*, no. 50. Stanford ,USA: The John A. Blume Earthquake Engineering Centre, 2006.

[22] G. Mylonakis, A. Nikolaou, and G. Gazetas, "Soil-pile-bridge seismic interaction: Kinematic and inertial effects. Part I: Soft soil," *Earthq. Eng. Struct. Dyn.*, vol. 26, no. 3, pp. 337–359, 1997, doi: 10.1002/(SICI)1096-9845(199703)26:3<337::AID-EQE646>3.0.CO;2-D.

[23] L. Tang, X. Ling, P. Xu, X. Gao, and D. Wang, "Shake table test of soil-pile groups-bridge structure interaction in liquefiable ground," *Earthq. Eng. Eng. Vib.*, vol. 9, no. 1, pp. 39–50, 2010, doi: 10.1007/s11803-009-8131-7.

[24] U.S. Geological Survey, "PEER Ground Motion Database," *Pacific Earthquake Engineering Research Centre*, 2018. [Online]. Available: https://ngawest2.berkeley.edu/.

[25] B. Wrana, W. Kalisz, and M. Wawrzonek, "Nonlinear Analysis of Pile Displacement Using the Finite Element Method," *Tech. Trans.*, vol. 2-B, pp. 137–147, 2013.

[26] C. J. Lee, M. D. Bolton, and A. Al-Tabbaa, "Numerical modelling of group effects on the distribution of dragloads in pile foundations," *Geotechnique*, vol. 52, no. 5, pp. 325–335, 2002, doi: 10.1680/geot.52.5.325.38704.

[27] C. A. T. Lucena, P. C. O. Queiroz, A. L. H. C. El Debs, and A. V. Mendonça, "Dynamic Analysis of Buildings Using the Finite Element Method," *Proc. 10th World Congr. Comput. Mech.*, no. May, pp. 4712–4726, 2014, doi: 10.5151/meceng-wccm2012-20033.

[28] S. Helwany, *Applied Soil Mechanics with ABAQUS Applications*, no. March. Hoboken, New Jersey: John Wiley & Sons; Inc., 2009.

[29] D. Pitilakis, M. Dietz, D. M. Wood, D. Clouteau, and A. Modaressi, "Numerical simulation of dynamic soil-structure interaction in shaking table testing," *Soil Dyn. Earthq. Eng.*, vol. 28, no. 6, pp. 453–467, 2008, doi: 10.1016/j.soildyn.2007.07.011.

[30] L. Šuklje, *Rheological aspects of soil mechanics.* London: Wiley-Interscience,A division of John Wiley & Sons Ltd, 1969.

[31] P. V. Lade, "Overview of constitutive models for soils," *Geotech. Spec. Publ.*, vol. 40771, no. 128, pp. 1–34, 2005, doi: 10.1061/40786(165)1.

[32] J. F. Labuz and A. Zang, *Mohr-Coulomb failure criterion*, vol. 45, no. 6. 2012.

[33] P. Menétrey and K. J. William, "Triaxial Failure Criterion for Concrete and its Generalization," *ACI Struct. J.*, vol. 92, no. 3, p. 311, 1995.

[34] A. N. Schofield, "Original Cam-clay," Guangzhou, 1993.

[35] O. Bezgin, "An insight into the influence of the construction Methods on the lateral load capacity of drilled deep foundations," in *4th ECCOMAS Thematic Conference on Computational Methods in Structural Dynamics and Earthquake Engineering*, 2014, no. 12–14 June, pp. 1–23, doi: DOI: 10.7712/120113.4821.C1024.

[36] H. Larew and G. A. Leonards, "A STRENGTH CRITERION FOR REPEATED LOADS," 1962.

[37] D. A. Sangrey, W. S. Pollard, and J. A. Egan, "Errors Associated With Rate of Undrained Cyclic Testing of Clay Soils.," in *Dynamic Geotechnical Testing*, M. L. Silver and D. Tiedemann, Eds. West Conshohocken, PA: ASTM International, 1978, pp. 280–294.

[38] A. Ansal and A. Erken, "Undrained Behavior of Clay Under Cyclic Shear Stresses," *J. Geotech. Eng.*, vol. 115, pp. 968–983, 1989.

[39] J. Zhou and X. Gong, "Strain degradation of saturated clay under cyclic loading," *Can. Geotech. J.*, vol. 38, no. 1, pp. 208–212, Feb. 2001, doi: 10.1139/t00-062.

[40] K. Yasuhara, K. Hirao, H. Fujiwara, and S. U-He, "Undrained Shear Behaviour of Quasi-overconsolidated Seabed Clay Induced by Cyclic Loading," *IDenness B. Seabed Mech.*, pp. 17–24, 1984, doi: https://doi.org/10.1007/978-94-009-4958-4_3.

[41] D. C. Procter and J. H. Khaffaf, "Cyclic Triaxial Tests on Remoulded Clays," *J. Geotech. Eng.*, vol. 110, no. 10, 1984, doi: https://doi.org/10.1061/(ASCE)0733-9410(1984)110:10(1431).

[42] A. F. L. Hyde, K. Yasuhara, and K. Hirao, "Stability Criteria for Marine Clay under One-Way Cyclic Loading," *J. Geotech. Eng.*, vol. 119, no. 11, p. ASCE, 1993, doi: https://doi.org/10.1061/(ASCE)0733-9410(1993)119:11(1771).

[43] M. Zergoun and Y. P. Vaid, "Effective stress response of clay to undrained cyclic loading," *Can. Geotech. J.*, vol. 31, no. 5, pp. 714–727, 1994, doi: 10.1139/t94-083.

[44] J. Liu and J. Xiao, "Experimental Study on the Stability of Railroad Silt Subgrade with Increasing Train Speed," *J. Geotech. Geoenvironmental Eng.*, vol. 136, no. 6, pp. 833–841, 2010, doi: 10.1061/(asce)gt.1943-5606.0000282.

[45] R. V Goldstein, A. V Dudchenko, and S. V Kuznetsov, "The modified Cam-Clay (MCC) model: cyclic kinematic deviatoric loading," *Arch. Appl. Mech.*, vol. 86, no. 12, pp. 2021–2031, 2016, doi: 10.1007/s00419-016-1169-x.

[46] D. A. Sangrey, D. J. Henkel, and M. I. Esrig, "THE EFFECTIVE STRESS RESPONSE OF A SATURATED CLAY SOIL TO REPEATED LOADING," *Can. Geotech. J.*, vol. 6, no. 3, pp. 241–252, Aug. 1969, doi: 10.1139/t69-027.

[47] S. F. Brown, A. K. F. Lashine, and A. F. L. Hyde, "Repeated load triaxial testing of a silty clay," *Géotechnique*, vol. 25, no. 1, pp. 95–114, Mar. 1975, doi: 10.1680/geot.1975.25.1.95.

[48] M. Vucetic and R. Dobry, "Degradation of Marine Clays Under Cyclic Loading," *J. Geotech. Eng.*, vol. 114, no. 2, pp. 133–149, 1988, doi: https://doi.org/10.1061/(ASCE)0733-9410(1988)114:2(133).

[49] H. B. Seed and C. K. Chan, "Clay Strength Under Earthquake Loading Conditions," *J. Soil Mech. Found. Div.*, vol. 92, no. 2, pp. 53–78, 1966.

[50] R. Iwahori, A., Hirota, Y., Sampe, "NII-Electronic Library Service," *Chem. Pharm. Bull.*, no. 43, p. 2091, 1970.

[51] H. Patiño, A. Soriano, and J. González, "Failure of a soft cohesive soil subjected to combined static and cyclic loading," *Soils Found.*, vol. 53, no. 6, pp. 910–922, 2013, doi: 10.1016/j.sandf.2013.10.010.

[52] B. K. Maheshwari, S. S. Kale, and A. M. Kaynia, "Effects of cyclic loads on dynamic properties of soils in the Ganga basin," *Int. J. Geotech. Eng.*, vol. 7, no. 2, pp. 149–155, 2013, doi: 10.1179/1938636213Z.00000000026.

[53] J. Jia, *Soil dynamics and foundation modeling: Offshore and earthquake engineering*, no. January 2018. 2017.

[54] J. Carter, J. Booker, and C. Wroth, "The application of a critical state soil model to cyclic triaxial tests," *Third Aust. Zeal. Conf. Geomech. Proc. Tech. Groups*, vol. 6, no. No 1 Part 1, pp. 121–126, 1980.

[55] J. P. Carter, J. R. Booker, and C. P. Wroth, "A critical state soil model for cyclic loading.," *Soils under Cycl. transient loading, Vol. 1. Proc. Int. Symp. Swansea, 7-11 January, 1980*, no. January 1982, pp. 433–434, 1982.

[56] J. Ni, B. Indraratna, X.-Y. Geng, J. P. Carter, and Y.-L. Chen, "Model of Soft Soils under Cyclic Loading," *Int. J. Geomech.*, vol. 15, no. 4, p. 04014067, 2015, doi: 10.1061/(asce)gm.1943-5622.0000411.

[57] Y. F. Dafalias, "The Concept and Application of the Bounding Surface in Plasticity Theory," in *Physical Non-Linearities in Structural Analysis*, 1981, pp. 56–63.

[58] K. I. Andrianopoulos, A. G. Papadimitriou, and G. D. Bouckovalas, "Bounding surface plasticity model for the seismic liquefaction analysis of geostructures," *Soil Dyn. Earthq. Eng.*, vol. 30, no. 10, pp. 895–911, 2010, doi: 10.1016/j.soildyn.2010.04.001.

[59] A. Stoecklin, B. Friedli, and A. M. Puzrin, "A multisurface kinematic hardening model for the behavior of clays under combined static and undrained cyclic loading," *Int. J. Numer. Anal. Methods Geomech.*, vol. 44, no. 17, pp. 2358–2387, 2020, doi: 10.1002/nag.3149.

[60] S. A. Whyte, H. J. Burd, C. M. Martin, and M. J. Rattley, "Formulation and implementation of a practical multi-surface soil plasticity model," *Comput. Geotech.*, vol. 117, no. January, 2020, doi: 10.1016/j.compgeo.2019.05.007.

[61] I. M. Idriss and J. I. Sun, *User's manual for SHAKE91 : a computer program for conducting equivalent linear seismic response analyses of horizontally layered soil deposits*. California , Berkeley: University of California, Davis. Center for Geotechnical Modeling.; Building and Fire Research Laboratory (U.S.).Structures Division., 1993.

[62] J. I. Sun, R. Golesorkhi, and H. B. Seed, "Dynamic Moduli And Damping Ratios for Cohesive Soils," 1990.

[63] M. Vucetic and R. Dobry, "Effect of Soil Plasticity on Cyclic Response," *J. Geotech. Eng.*, vol. 117, no. 1, pp. 89–107, 1991.

[64] G. Mylonakis and G. Gazetas, "Seismic soil-structure interaction: Beneficial or detrimental?," *J. Earthq. Eng.*, vol. 4, no. 3, pp. 277–301, 2000, doi: 10.1080/13632460009350372.

[65] M. R. Ashory, "High Quality Modal Testing Methods," Imperial college University London, 1999.

[66] P. M. Byrne, S. Park, M. Beaty, and M. Sharp, "Numerical Study of The Soil-Structure Interaction During Strong Earthquakes," in *13th World Conference on Earthquake Engineering*, 2004, no. Paper No. 2959.